Proc. of SPIE Vol. 0450, Structural Mechanics of Optical Systems I, ed. L.M. Cohen (Jan 1983) Copyright SPIE

Uses and abuses of the finite element method

Oscar Orringer and Pin Tong

U.S. Department of Transportation
Transportation Systems Center
DTS-76, Kendall Square
Cambridge, MA Ø2142

Abstract

Almost three decades of advances in theory and software together with the development of large-scale mainframe computers have put the finite element method at the fingertips of the structures design/analysis engineer. Ten of those years have included mechanization and automation of the design process, a trend which continues today. The ability to rapidly design complex structures is the positive result of this trend. However, there is also a negative aspect, viz: structures engineers can lose sight of the facts that the finite element model is only a model and that it may exclude the most significant mechanical characteristics of the real structure.

This paper is based on the authors' experience with both theory and applications. Numerous examples are drawn upon to illustrate both the utility of the finite element method and its propensity, when abused, to produce numbers which look plausible but are actually wrong. The paper concludes with some guidelines for finite element modelling of structural systems and details.

Introduction

The finite element method predates the modern digital computer by a decade. Courant used elements based on a stress function to calculate approximate solutions of the St. Venant torsion problem in the early 1940's.[1]

In the mid-195Ø's the aircraft industry began to apply matrix structural analysis to the computation of airframe flight stresses. Second-generation digital computers (one hundred thousand data words in core RAM, one million floating-point arithmetic operations per second) and sparse-matrix equation-solving techniques were the key factors which made the application practical.

The early airframe analyses were based on panel-and-stringer models in which the panel elements were simple constant-shear skins, while the stringers were one-dimensional tension/compression members, possibly with shear-lag effects included. Finite element programs of this type are still in wide use because they provide a reasonable engineering representation of the thin stressed-skin construction of typical airframes.

The aircraft work in the 195Ø's also stimulated the development of more sophisticated elements to deal with variable skin thickness, beam and plate bending effects, and continua in either plane elasticity or three dimensions. Energy theorems based on the variational calculus approach to mechanics began to be used to develop the new elements. By the early 196Ø's many different elements were available based on assumed displacement fields and the Principle of Minimum Potential Energy. Engineers outside the field of aeronautics were beginning to express interest in finite element analysis, but the ad hoc nature of most of the programs then available made application difficult.

From the late 196Ø's to the mid-197Ø's the demand for software stimulated the development of general-purpose programs in FORTRAN with batch-mode input, in "user-oriented" languages, and ultimately in terminal/interactive mode with CRT display of the model grid. In the same period advanced variational mechanics was used to extend the finite element method to models based on the Principle of Minimum Complementary Energy, Reissner's Principle, etc., and elements based on assumed stress fields or combination of assumed stresses and assumed displacements appeared.

Today there exists a wide variety of elements and general-purpose programs to choose from, including many programs with CRT-interactive input. Using the finite element method is now so easy that junior engineers can be trained as model-makers/analyzers with little more effort than imparting the rules about how to run a specific program. This situation may appeal to the engineering supervisor faced with a need to rapidly analyze a complex structural part, and it is of genuine benefit in today's environment of limited budgets.

However, such computational plenty has a high price if junior engineers analyze complex

parts without understanding the basic theory and limitations of the method. Beyond some conventional notions about convergence (more elements improve accuracy), the analyst must understand the rules for good model-making, how to interpret results from a crude model, how different kinds of elements perform (including nonconvergent behavior), and how complex structural systems and/or finite-digit floating-point arithmetic can create subtle traps when everything else appears to be right.

Textbooks are the starting point for such understanding. Many books are available today on the fundamentals of the assumed-displacement approach with a few basic elements[2-4], on advanced assumed-displacement elements with extensive detail on numerical integration and stiffness matrix formation[5,6], on the mathematics of the finite element method[7],and on advanced elements based on different variational principles.[8,9] For the most part, however, these books concentrate on the derivation of stiffness matrices and the performance of elements in idealized test conditions. Papers on the practical aspects of model/computer behavior are scattered in the literature, making it difficult for the analyst to grasp the important limitations and traps which exist.

This paper is intended to provide a reference on practical aspects of the finite element method. Only elastic behavior is covered because the practicing engineer's main concern is to design structures that do not yield or fail in service. The body of the paper includes a collection of cases with which the authors were directly or indirectly involved over a decade of research and application experience. The cases have been selected to illustrate both abuse and effective use of the finite element method. We hope that future analysts will benefit by not having to learn these lessons by trial and error. The paper concludes with some guidelines for good practice. It is worthwhile, however, to state one guideline immediately. Every analyst should have a good stress analysis handbook[10] in his library and should be ready to use it in lieu of or as a supplement to computer analysis.

Aspect ratio

The aspect ratio of a rectangular element of sides AxB (A > B) is defined as $\alpha = A/B$. Analogous definitions exist for triangles, quadrilaterals, and the corresponding solid elements. It is desirable to keep element aspect ratios as close to unity as possible, but some elements usually have to be stretched to fit a grid onto a complex-shaped part. However, there are two limits on the amount of stretch that can be tolerated.

The upper limit is associated with kinematic instability, as shown by considering the rectangular plane-stress element. The element stiffness matrix in this case is:

$$\underset{\sim}{k} = \left(\frac{Et}{12(1-\nu^2)}\right)\begin{bmatrix} 4/\alpha+2(1-\nu)\alpha & & \text{(Symmetric)} & \\ 3(1+\nu)/2 & 4\alpha+2(1-\nu)/\alpha & & \\ 2/\alpha-2(1-\nu)\alpha & 3(1+\nu)/2 & 4/\alpha+2(1-\nu)\alpha & \\ \cdot & \cdot & \cdot\ \cdot & \\ \cdot & \cdot & \cdot\quad\cdot & \\ \cdot & \cdot & \cdot\qquad\cdot & \\ \cdot & \cdot & \cdot\qquad\qquad\cdot \end{bmatrix} \tag{1}$$

where E is Young's modulus, ν is Poisson's ratio, and t is the element thickness. For large aspect ratios the α-terms in Eq. 1 dominate $\underset{\sim}{k}$:

$$\lim_{\alpha\to\infty}(\underset{\sim}{k}) = \left(\frac{Et\alpha}{12(1-\nu^2)}\right)\begin{bmatrix} 2(1-\nu) & & \text{(Symmetric)} & \\ 0 & 4 & & \\ -2(1-\nu) & 0 & 2(1-\nu) & \\ \cdot & \cdot & \cdot\ \cdot & \\ \cdot & \cdot & \cdot\quad\cdot & \\ \cdot & \cdot & \cdot\qquad\cdot & \\ \cdot & \cdot & \cdot\qquad\qquad\cdot \end{bmatrix} \tag{2}$$

i.e. the effect of the xy cross-coupling terms $3(1+\nu)/2$ is lost, and the element becomes unstable in shear. Attempts to solve a uniformly stretched grid will fail by kinematic singularity in the assembled stiffness matrix if the aspect ratio is large enough.

Below the kinematic limit there exists a performance limit which depends on the order of the element's assumed displacement field and the expected displacement gradients, as well as

the aspect ratio. Extensive study of the plane-stress bilinear rectangle element has shown, for example, that the element's assumed displacement field cannot accurately follow the quadratic transverse displacement gradient along the axis of a cantilever beam loaded by a concentrated end moment when the element aspect ratio exceeds three.[2] We have performed similar tests to show that 8-node biquadratic rectangles are able to solve the moment-loaded cantilever beam at any aspect ratio below the kinematic limit, but cannot follow the cubic gradient caused by a transverse end load when the aspect ratio exceeds about seven.

We have also tested 8-node trilinear, 20-node triquadratic, and 32-node tricubic isoparametric hexahedra in the course of developing software for three-dimensional analysis of gear teeth.[11] These studies showed that the 8-node hexahedron cannot be trusted above an aspect ratio of two. Also, the 20-node hexahedron was found to be the best compromise for analyzing complex three-dimensional shapes when model size (total degrees of freedom), geometric matching requirements at boundaries, and relative computing burden were considered. The higher-order elements decrease model size because of better aspect ratio performance and are easier to fit into fillet or radius details, but they increase the computing time required to form the element stiffness matrices. On one hand, models with 8-node hexahedra required excessively large size and global computing time to keep the element aspect ratios within acceptable limits. On the other hand, the sizes of models with 32-node hexahedra tended to be bounded from below by the number and location of details in the part, and the extra computing time required to form the element stiffnesses exceeded the savings in global computing time.

Element shape

The option of distorting higher-order isoparametric element shapes provides a convenient way to fit curved boundaries with a few elements. Excessive distortion can ill-condition the element stiffness matrix, however, leading to inaccurate results.

The nodal coordinates of an isoparametric element are interpolated in the same way as the nodal displacements.[6] For example, a generalized quadrilateral plane-stress element is described by:

$$\begin{aligned} x &= \underset{\sim}{B}(\xi,\eta)\,\underset{\sim}{X} \quad ; \quad y = \underset{\sim}{B}(\xi,\eta)\,\underset{\sim}{Y} \\ u &= \underset{\sim}{B}(\xi,\eta)\,\underset{\sim}{q}_x \quad ; \quad v = \underset{\sim}{B}(\xi,\eta)\,\underset{\sim}{q}_y \end{aligned} \tag{3}$$

where (x,y) and (u,v) are the internal coordinates and displacement fields, respectively, $\underset{\sim}{X}$ and $\underset{\sim}{Y}$ are the nodal coordinates, $\underset{\sim}{q}_x$ and $\underset{\sim}{q}_y$ are the nodal displacements, and $\underset{\sim}{B}$ contains the interpolations given in terms of "parent" coordinates (ξ,η) in which the element edges lie along $(\xi,\eta) = \pm 1$. The values of $\underset{\sim}{X}$,$\underset{\sim}{Y}$ and the order of the polynomials in $\underset{\sim}{B}$ determine the shapes of the element edges in the physical (x,y) plane.

The element stiffness matrix is computed by expressing the strain energy density in terms of $\partial u/\partial x$, $\partial u/\partial y$, $\partial v/\partial x$, $\partial v/\partial y$ and numerically integrating over the element area. Since (u,v) are interpolated in terms of (ξ,η), however, the strains must be computed indirectly and the Jacobian transformation must be used:

$$\begin{Bmatrix} \partial(\,)/\partial x \\ \partial(\,)/\partial y \end{Bmatrix} = \underset{\sim}{J}^{-1} \begin{Bmatrix} \partial(\,)/\partial \xi \\ \partial(\,)/\partial \eta \end{Bmatrix} \tag{4}$$

where

$$\underset{\sim}{J} = \begin{bmatrix} \partial x/\partial \xi & \partial y/\partial \xi \\ \partial x/\partial \eta & \partial y/\partial \eta \end{bmatrix} = \begin{bmatrix} (\partial \underset{\sim}{B}/\partial \xi)\,\underset{\sim}{X} & (\partial \underset{\sim}{B}/\partial \xi)\,\underset{\sim}{Y} \\ (\partial \underset{\sim}{B}/\partial \eta)\,\underset{\sim}{X} & (\partial \underset{\sim}{B}/\partial \eta)\,\underset{\sim}{Y} \end{bmatrix} \tag{5}$$

Also, the area integration is carried out in accordance with:

$$\iint_A (\,)\,dx\,dy = \int_{-1}^{+1}\int_{-1}^{+1} (\,)\left|\mathrm{Det}(\underset{\sim}{J})\right| d\xi\, d\eta \tag{6}$$

Moderate shape distortions cause no problem, but excessive distortions can ill-condition the Jacobian matrix $\underset{\sim}{J}$, introducing spurious behavior in the strain fields. For example, $\underset{\sim}{J}$ is singular if the quadrilateral is degenerated to a triangle by allowing the locations of two nodes two coincide. The transformation of distortions causes so much error that it is

not worthwhile to model sharply curved boundaries with too few higher-order elements.[8] It is generally advisable to keep the lengths of an element's edges within a ratio of 4:1 and to avoid curvatures which offset the mid-edge node further than 30 percent of the edge chord.

One should exercise similar caution when using distortable hybrid elements. Although in this case the direct assumption of internal stress fields eliminates the need for a Jacobian transformation of derivatives, the volume integration still follows Eq. 6 and may be affected by errors in Det($\underset{\sim}{J}$).

The patch test

Since the equations governing plates and shells involve fourth order differentiations, interpolation functions and their normal slopes are generally required to be continuous at the element boundaries to maintain interelement compatibility. However, it is sometimes difficult to find simple interpolation functions which satisfy all the compatibility conditions. Hence, many incompatible (nonconformal) elements have been developed, usually by ignoring the normal slope continuity requirement. These elements often produce reasonable results when they are tested in a coarse grid on a simple problem with a known solution. However, there are cases in which the finite element solutions actually converge to wrong answers.

A famous example is the nine-degree-of-freedom triangular element employing a complete cubic polynomial as the interpolation function (see Figure 1). Since a complete cubic polynomial has ten terms, either a judiciously selected term is dropped or static condensation is used to reduce the ten freedoms to nine. The reduced interpolation assures displacement continuity along the interelement boundary, but the normal slopes are continuous only at the nodes.

Bazeley et al.[12] tested this element in two grid patterns to solve the problem of a centrally loaded square plate (Figure 2) and found that pattern B gave a wrong answer. This led to the patch test for nonconformal elements, i.e. when a number of such elements are assembled in a patch, the patch must be able to represent all the constant-strain deformations over its domain. Pattern B in Figure 2 does in fact fail the patch test. Strang and Fix[7] later proved that passage of the patch test assures the convergence of nonconformal elements.

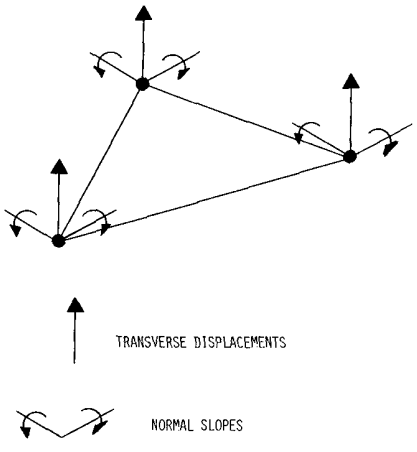

Figure 1. Triangular plate bending element

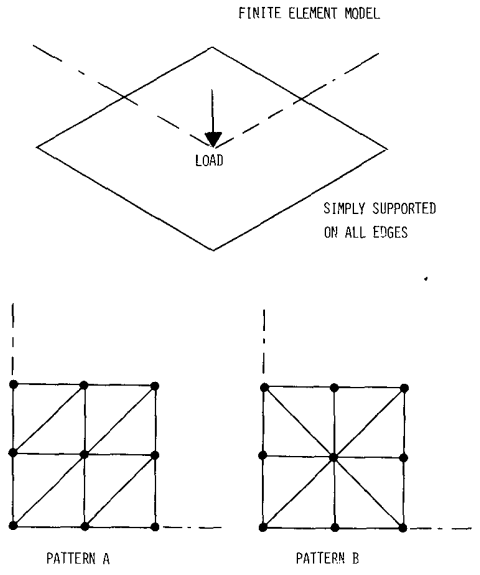

Figure 2. Element performance test

Nonconformal elements are generally simpler than conformal elements and, as mentioned earlier, give reasonable results. Nonconformal elements also impose fewer constraints on the interpolation functions and, therefore, are generally more flexible than comparable conformal elements, i.e. the nonconformal elements may produce more accurate solutions if properly converged. However, the proposed grid pattern should always be patch-tested to assure proper convergence before nonconformal elements are used in a practical application.

Problems with singularity

Polynomial interpolation functions have been successfully and widely used for practical finite element applications. Polynomials are simple to manipulate on the computer, they can easily be chosen to assure the satisfaction of interelement compatibility conditions, and one can either refine the grid by reducing the element sizes or use higher-order polynomials to improve the solution accuracy. The basic premise of such finite element methods is that all smooth functions look like polynomials in a sufficiently small region, i.e. the polynomial representation of a function can be improved if the region is made smaller or the order of the polynomial is increased. This situation may not be true if the solution to be approximated has a singularity or if the domain of the problem is infinite. In the first case, it is clear that a polynomial cannot represent the function near its singular point. In the second case, at least one of the elements must have an infinite size. The infinite-domain situation will be discussed in a later section in conjunction with a wave propagation problem.

One of the most commonly encountered singularities in solid mechanics is of the type r^{λ}. For example, the displacement u near the tip of a re-entrant corner (notch) in a plane elasticity problem is:

$$u \sim r^{\lambda} \tag{7}$$

where r is the distance from the notch tip and λ is in general a complex number. For the special case that the notch is a crack, $\lambda = 1/2$, while $1/2 < \mathrm{Re}(\lambda) < 1$ for a finite-angle notch when the included angle lies between Ø and 18Ø degrees.[13,14] It is obvious that polynomials cannot represent u at or near r = Ø.

Comparison of the computed and exact strain energies for a problem is a convenient way to measure the rate of convergence of the approximate solution because the finite element method is often based on strain energy. It has been shown for singular problems[15] that the convergence rate is proportional to $h^{2\mathrm{Re}(\lambda)}$, where h measures the element size. This is contrary to the conventional wisdom[7,16] that the convergence rate follows h^{2n}, where n is the order of the interpolation polynomial. In other words, the singularity controls the convergence rate. In the case of a crack the convergence rate is thus only proportional to h. Conversely, the convergence rate is proportional to h^2 when the simplest linear-interpolation elements are used to model unnotched domains.

Since polynomials cannot approximate a singularity, it is crucial to understand that conventional elements will produce ever-increasing stresses near the singular point as the element size is reduced. Such results are difficult to interpret unless the order of the singularity is known a priori. Even then the slow convergence rate can still impose limits on the attainable computational accuracy because computer capacity and/or roundoff error may limit the extent to which the grid can be refined.

These limitations can be removed by selecting an interpolation function which accounts for the singular behavior. The successful techniques based on this approach include: isoparametric elements with quarter-point nodes on the element boundaries at the crack tip[17]; using the J-integral theorem to compute stress intensity factors from the finite element solution[18]; including functions with proper singularity but otherwise smooth over the entire domain[19]; and the hybrid finite element technique.[20]

Tests of conventional elements have been compared with tests of hybrid singularity elements on the symmetrical edge-crack problem to demonstrate the drastic accuracy improvement the hybrid approach provides. Figure 3 compares the rate of convergence of strain energy for the two methods applied to grids of identical element size. Although the hybrid singular elements surrounding the crack tips require more time to form the element stiffness matrices, overall computational efficiency is greatly improved.

The hybrid technique has been extensively applied to compute the stress intensity factors at airframe construction details.[21-24] Figure 4 illustrates a representative case involving side-bearing loads applied to the aft engine attachment lug of the C-5A airframe. Each result is a polar plot of the Mode I and Mode II stress intensity factors which correspond to 32 different angular locations of the crack. Each data point required about 2 CPU seconds on an IBM S-370/168.

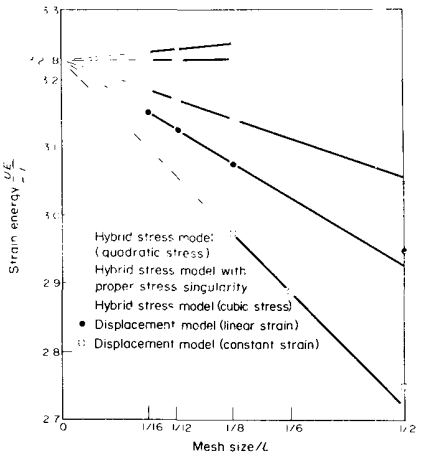

Figure 3. Comparison of strain-energy convergence rates

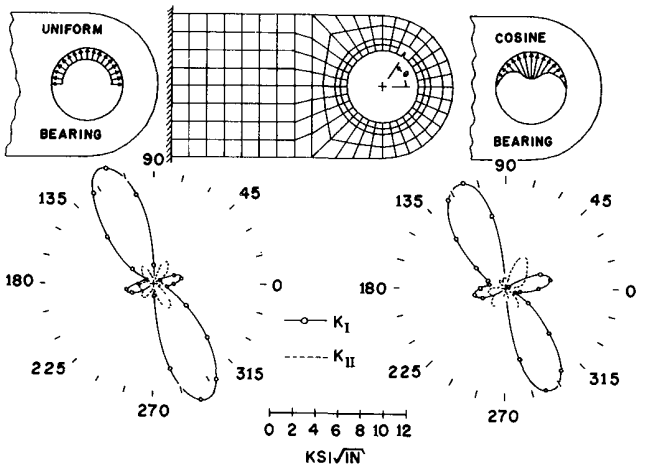

Figure 4. Attachment lug finite element model and results

Theoretical overkill

The "solution looking for a problem" is sometimes a byproduct of theoretical mechanics, especially in today's environment where basic research budgets have to be justified in terms of immediate applications. Unfortunately, it is often all too easy for such byproducts to be disguised in computer programs that are advertised as means to analyze stresses in structures which do not conform to the assumptions of the theory.

The following singularity problem illustrates how easy it is to lose sight of theoretical quirks in the rush to apply a solution. A manufacturer of printing press rollers, having found the rubber cover debonding from the metal structure in a new design, requested that a laboratory test be developed to measure debonding rates under fatigue loads and chemical environments simulating roller service. One approach involved a variation on the compact tension specimen to induce a debond crack to grow under alternating shear stress (Figure 5), and required a stress singularity in the analysis of the test specimen.[25] The finite element model included a hybrid element (SKBP17) which specifically accounted for the singularity at a crack along the interface of two dissimilar elastic materials (Figure 6) and produced apparently reasonable solutions for the corresponding stress intensity factors (Figure 7).

Given the facility of the finite element method, it is tempting to leap from the foregoing results to a program of laboratory crack growth rate tests correlated with the debond stress intensity factor and finite element calculations of stress intensity factors for debonds at production details in the roller. However, the singularity associated with the debond crack involves Bessel functions in both the stress displacement fields. In particular, the displacement across the bond line oscillates, and the crack surfaces can overlap in the model even when the computed stress intensity factor is positive. Such solutions are obviously irrelevant to the physical problem, which was ultimately solved by means of engineering analyses and simpler experiments.

The analysis of stresses in laminated fiber composites presents a more subtle case. Although the interior stresses are well described by the theory of orthotropic laminated plates and the corresponding finite elements[26], the stress field includes interlaminar components in zones of the order of the laminate thickness near free edges,[27,28] and experiments have shown that composite plates can fail by means of combined interlaminar shear and tension in the edge zone.[29] Much effort has consequently been spent on theoretical analysis and development of special elements to deal with laminate edge-zone

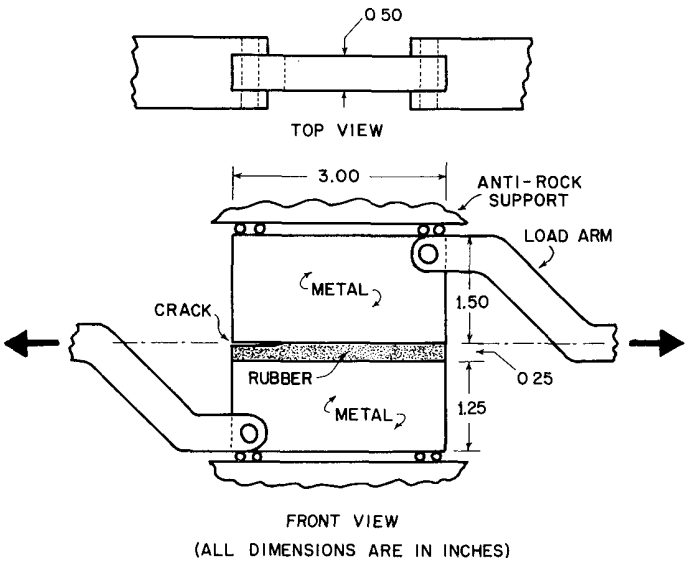

Figure 5. Debond test specimen configuration

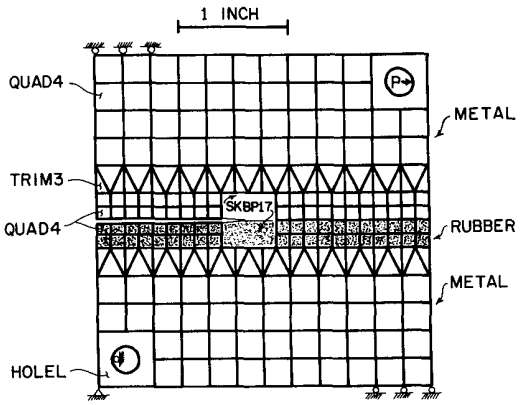

Figure 6. Specimen finite element model

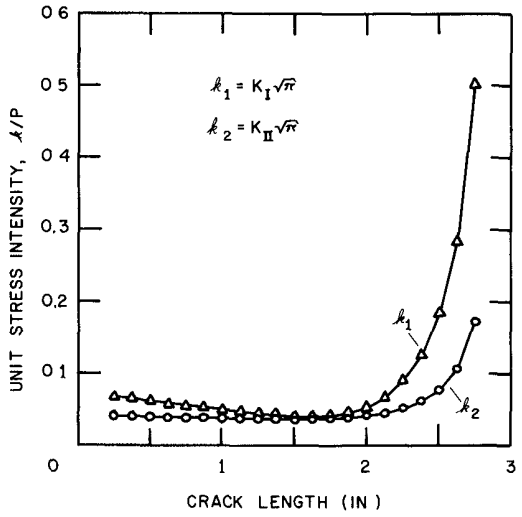

Figure 7. Computed stress intensity

effects (for example, see Section 17.7 of Reference 9 for details). All of these models assume that the laminate consists of homogeneous orthotropic layers with discrete changes of elastic constants at the interlayer boundaries. However, the regions of significant interlaminar stress are usually confined to distances of the order of a few fiber diameters, i.e. a scale at which the material should be modelled as a two-phase isotropic fiber/resin system.

Infinite domains

One is naturally inclined to treat an infinite-domain problem by means of a model posessing a finite but sufficiently large domain, i.e. one implicitly assumes that the influence of distant boundaries is negligible. The intuition that whatever happens locally cannot affect distant points and vice versa is usually satisfactory if the problem is governed by elliptic equations, such as the equations of solid mechanics. Erroneous answers will result, however, when hyperbolic problems such as wave propagation are addressed.

The stress wave in a semi-infinite rod ($x \geq 0$) subjected to a suddenly applied load at one end ($x = 0$) is a simple example. The governing equation is:

$$\partial^2 u / \partial x^2 = c^2 \, \partial^2 u / \partial t^2 \tag{8}$$

and the exact solution is of the form:

$$u = f(x-ct) \tag{9}$$

where c is the wave propagation speed. However, if one attempts to solve such a problem by

a finite element model with a boundary condition at a finite distance, reflected waves will appear in the numerical solution, which then has no resemblance to the exact solution of the original problem.

Another example is the propagation of disturbances at the free surface of a flow in a two-dimensional channel.[30] The flow behavior is controlled by the nondimensional Froude number:

$$F = V^2/gH \tag{10}$$

where V is the freestream flow speed, g is the acceleration of gravity, and H is the depth of the fluid. All disturbances die down in a finite distance when $F < 1$, and the imposition of approximate boundary conditions distant from the disturbances will produce adequate results. If $F > 1$, however, there is no dissipation mechanism in the mathematical model to damp out the disturbance, and one cannot expect to obtain a correct or nearly correct solution without accounting for the finite amplitude of the disturbance at any finite distance downstream. One can argue that some dissipation is always present in the flow of a real fluid and, therefore, that a model with dissipation and a finite boundary at a correspondingly suitable distance can always be employed. However, the physical situation is often such that this boundary must lie far away from the region of interest where waves propagate and reflect at nearby physical boundaries. In such cases it is computationally more efficient to neglect the dissipation and to use an infinite-domain model.

In order to assure that the infinite-domain approximation is correct, one must properly account for the so-called radiation condition, which describes how the disturbance propagates to the far field. One approach is to divide the domain into near and far field regions.[8,30] The near field region is sufficiently large to enclose all the locations of interest, while the far field region encompasses the rest of the domain. The near field region is subdivided into a finite number of conventional elements in the usual way. However, the far field region is left as one element which includes the proper asymptotic solution in its interpolation functions. The element interpolation functions are matched at the inter-region boundary by a hybrid finite element technique.[8] Some numerical examples can be found in Reference 30.

Interpretation of nodal forces

There is usually no confusion about the representation of applied loads by nodal forces on finite element models, but some ambiguities require careful interpretation. Nodal point forces or distributions of nodal forces over a few elements do not always represent the equivalent point or distributed applied loads.

For example, consider a typical edge of a linear-interpolation plane-stress element assumed to be loaded by a distributed force p(x), which is to be represented by nodal forces Q_1, Q_2 at the corner nodes (see Figure 8). The corresponding edge displacement field u(x) is related to the nodal displacements q_1, q_2 by:

$$u(x) = \underset{\sim}{q}^T \underset{\sim}{B}(x) = \begin{bmatrix} q_1 & q_2 \end{bmatrix} \begin{Bmatrix} 1-x/\ell \\ x/\ell \end{Bmatrix} \tag{11}$$

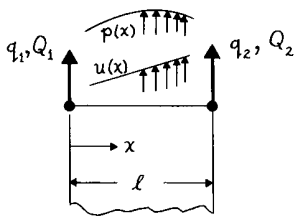

Figure 8. Typical edge of plane-stress element

The nodal forces are derived by substituting Eq. 11 into the Principle of Virtual Work[9] for the edge,

$$\underset{\sim}{q}^T \underset{\sim}{Q} = \int_0^{\ell} u(x)\,p(x)\,dx = \underset{\sim}{q}^T \int_0^{\ell} \underset{\sim}{B}(x)\,p(x)\,dx \tag{12}$$

and "cancelling" $\underset{\sim}{q}^T$ because Eq. 12 must hold for any values of the displacements:

$$\begin{Bmatrix} Q_1 \\ Q_2 \end{Bmatrix} = \int_0^{\ell} \begin{Bmatrix} (1-x/\ell)\,p(x) \\ (x/\ell)\,p(x) \end{Bmatrix} dx \tag{13}$$

In particular, for a linear load distribution such that $p(0) = p_1$ and $p(\ell) = p_2$:

$$\begin{Bmatrix} Q_1 \\ Q_2 \end{Bmatrix} = \begin{bmatrix} 1/3 & 1/6 \\ 1/6 & 1/3 \end{bmatrix} \begin{Bmatrix} p_1\ell \\ p_2\ell \end{Bmatrix} \tag{14}$$

Now consider the special case $(p_1,p_2) = (2p,-p)$, for which Eq. 14 leads to:

$$Q_1 = p\ell/2 \quad ; \quad Q_2 = \emptyset \tag{15}$$

It is apparent from Eq. 15 that a point force Q at a node joining two linear-interpolation elements can be interpreted as the triangular load distribution shown in Figure 9A. One might be tempted to think of Q as representing a concentrated load $p(x) = Q\delta(x)$, where δ is the Dirac function (Figure 9B), but the element interpolation cannot produce stress gradients steeper than the linear result one would expect from the Figure 9A loading. Hence, the stress solution near a plane-stress point nodal force on conventional elements cannot be interpreted as the stress which a concentrated load would cause. Hybrid elements with singular stress terms corresponding to the Boussinesq problem are required to correctly compute stresses near concentrated loads on continuum finite element models.

A similar problem arises in dealing with the end-points of distributed loads. For example, a uniform load $p_1 = p_2 = p$ leads to nodal forces $Q_1 = Q_2 = p\ell/2$ for the typical element. Thus, a uniform distribution is represented by $Q,2Q,2Q,\ldots,2Q,Q$ (Figure 1ØA). No ambiguity arises if the loading spans an entire boundary of the structure, but the finite element model approximates a mid-boundary load discontinuity as a linear load reduction (Figure 1ØB), and the local stress solution again follows the approximation.

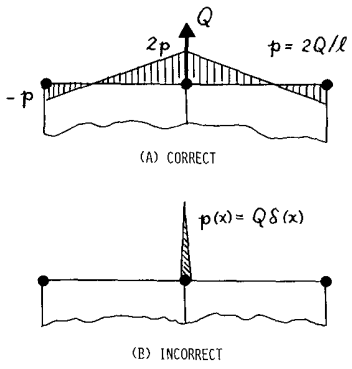

Figure 9. Interpretations of a point nodal force

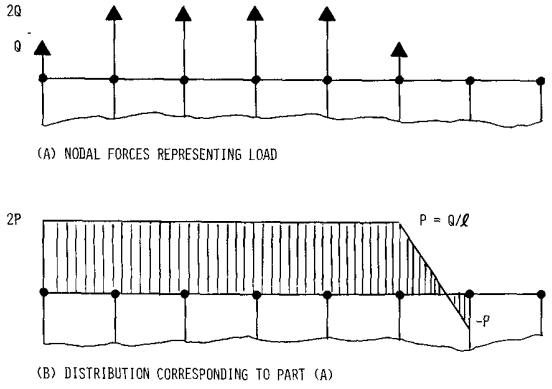

Figure 1Ø. Nodal force approximation of sharply cut-off load

Roundoff error

Increasing the number of elements to refine a grid for better convergence is a well known tactic. However, the floating-point rounding operation in a digital computer limits the attainable accuracy. The limit is of no concern for modest-size grids, but it lurks in wait for the unwary analyst who has access to a large computer and naive faith in the efficacy of large numbers of small elements.

Roundoff error is part of the total error, which can be measured in a mean square sense as follows. Let:

$$\Delta u_j = u_j(\text{exact}) - u_j(\text{computed}) \quad ; \quad j = 1,2, \ldots ,J \tag{16}$$

be the individual errors in the nodal displacements of a J-degree-of-freedom model, and define the RMS error:

$$\mathcal{E} = \sqrt{\left(\sum \Delta u_j^2\right)/\left(\sum u_j^2(\text{exact})\right)} = \mathcal{E}_C + \mathcal{E}_R \tag{17}$$

Convergence error $\mathcal{E}_C$ ordinarily dominates $\mathcal{E}$, but $\mathcal{E}_C$ decreases and the roundoff error $\mathcal{E}_R$ begins to dominate as the grid is refined. The RMS roundoff error can be estimated a priori from:[31]

$$\log_{1\emptyset}(\mathcal{E}_R) = -p + A[\log_{1\emptyset}(BN^d)] \tag{18}$$

where p is the computer precision in decimal places, N is the maximum number of elements along one edge of the model, d is the order of the field equations on which the elements are based, and A,B are model-dependent constants. For plane-stress/plane-strain and solid

elements d = 2; for beam and plate-bending elements d = 4. For practical purposes $A \approx 1$, and:

$$B \sim \lambda_{MAX}/\lambda_{MIN} \tag{19}$$

where λ_{MAX} is the largest eigenvalue of any individual element stiffness matrix in the model and λ_{MIN} is the smallest eigenvalue of the model's assembled stiffness matrix. It is apparent from Eqs. 18 and 19 that grid refinement accelerates the growth of $\mathcal{E}_R$, i.e. both N and B increase. (B increases because λ_{MAX} increases as the element sizes decrease, while λ_{MIN} is constant for a given global model and boundary conditions.) No general proof exists for the behavior of individual errors, but one must intuitively conclude that they should follow the trend of the RMS error.

We have used the four-degree-of-freedom cubic-displacement beam element (Figure 11) to demonstrate the roundoff effect on individual errors. It is easy to show from the element stiffness matrix,

$$\underset{\sim}{k} = (EI/\ell^3)\begin{bmatrix} 12 & & \text{(Symmetric)} & \\ 6\ell & 4\ell^2 & & \\ -12 & -6\ell & 12 & \\ 6\ell & 2\ell^2 & -6\ell & 4\ell^2 \end{bmatrix} \tag{20}$$

that a one-element model gives the exact beam-theory solution:

$$\delta = P\ell^3/3EI \tag{21}$$

for the tip deflection of a cantilever beam subjected to a tip load P. Similar proofs can be given for any case of concentrated loading, and hence $\mathcal{E} = \mathcal{E}_R$ for finite element models of such beams.

Figure 12 summarizes the results of some numerical experiments with cantilever and simply supported beams, showing the effect of roundoff on the computed tip and mid-span deflections, respectively. The calculations were performed in single precision on an IBM S-370/165 (p = 7.2 decimal places). The bounds $\mathcal{E} = 1$ denote 100 percent error. Changes occur in the error details as variations in the element length change the values of A,B, and λ_{MAX}, but each model has a more or less constant value for the number of elements at which the error bound is reached.

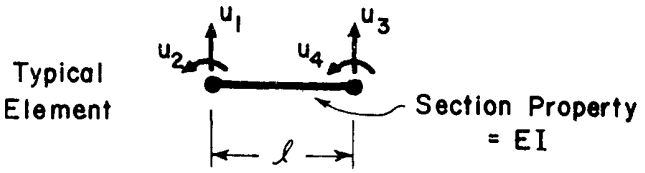

Figure 11. Beam element

Figure 13 illustrates an example of an error that really counts: the computed bending moment diagram. If the analyst's theoretical knowledge were limited to the general idea that one should look near the support to find the maximum bending moment, he might accept a result which is one fourth of the true value in this case. The beam illustration is academic, but there are real pitfalls in using continuum models to compute stress (the continuum analog of the beam bending moment), for example, at a radius detail in a complex part for which no analytical solution exists. Evaluation of plane continuum elements has shown that[32] the critical value of N is about 25 to 30 elements per edge when p = 7.2 decimal places[32], and similar behavior should be expected for solid elements.

Fortunately, one can avoid excessive roundoff error by increasing precision from p_1 to p_2, thereby increasing the critical number of elements per edge from N_1 to:

$$N_2 = N_1[10^{(p_2 - p_1)}]^{1/d} \tag{22}$$

If the continuum case ($p_1 = 7.2$, $N_1 = 25$, $d = 2$) is taken as the baseline, Eq. 22 shows that typical scientific mainframes ($p_2 = 10.3$) give $N_2 \approx 800$. Even business machines are satisfactory if double-precision arithmetic is used ($p_2 = 14.2$, $N_2 \approx 8{,}000$).

The roundoff error arises during solution of the global force-displacement relations when the stiffness matrix $\underset{\sim}{K}$ is factored. For example, suppose that Gauss triple factoring is used:

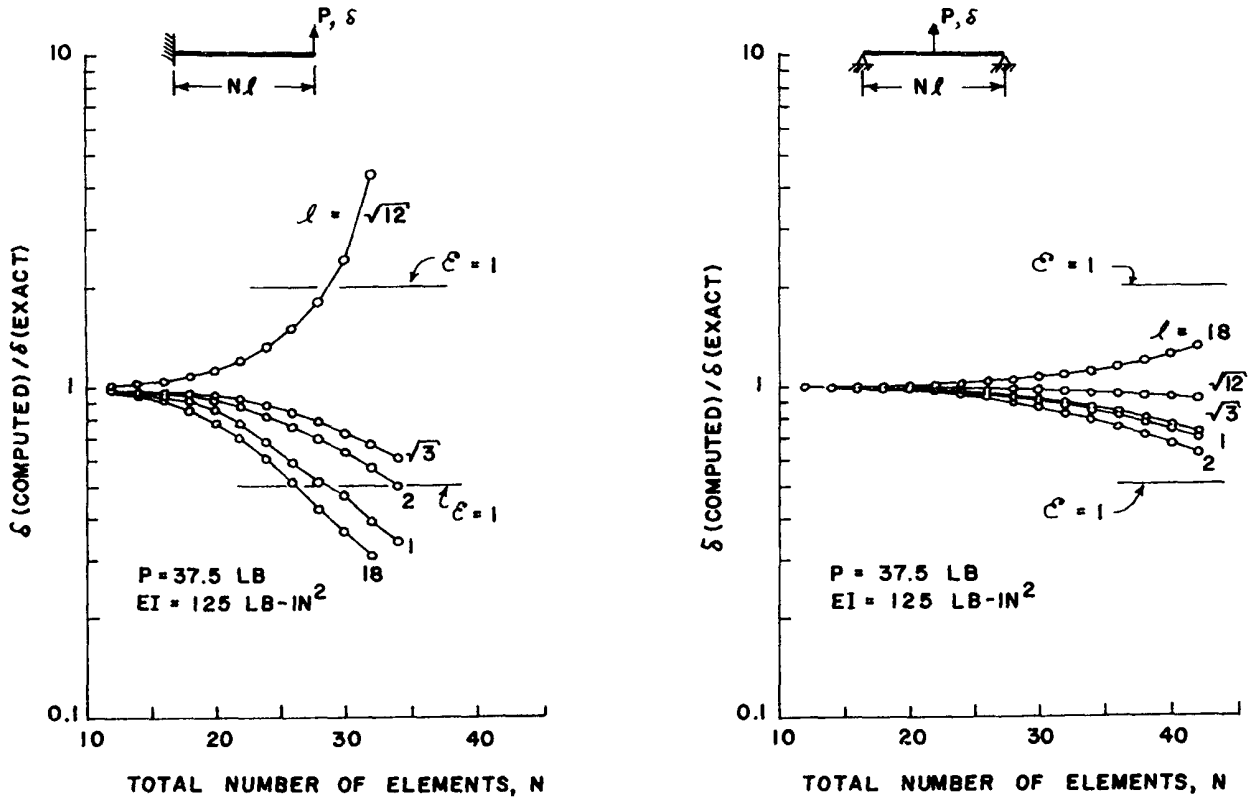

Figure 12. Illustration of roundoff error in computed beam deflections

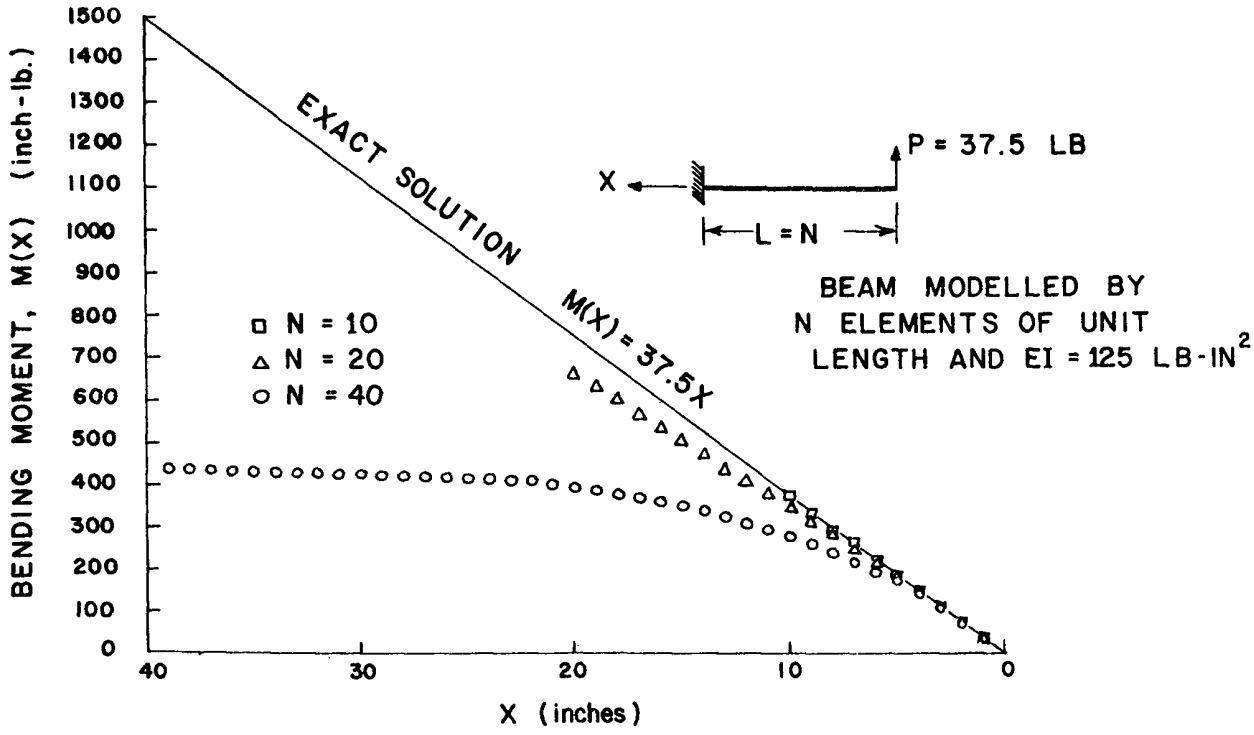

Figure 13. Illustration of roundoff error in computed bending moment

$$\underset{\sim}{K} = \underset{\sim}{L}\underset{\sim}{D}\underset{\sim}{L}^{T} \tag{23}$$

where the factors $\underset{\sim}{L}$ and $\underset{\sim}{D}$ are respectively a lower-triangular matrix with unit values on the diagonal and a diagonal matrix. The coefficients of the factors are:

$$L_{mn} = (K_{mn} - \sum_{j=1}^{n-1} D_{jj} L_{mj} L_{nj})/D_{nn} \quad ; \quad n = 1,2,\ldots,m-1 \tag{24}$$

$$D_{mm} = K_{mm} - \sum_{j=1}^{m-1} D_{jj} (L_{mj})^2 \quad ; \quad m = 1,2,\ldots,J \tag{25}$$

Equation 25 shows that information can be lost from the diagonal coefficients when large numbers are subtracted to produce small differences. The resulting error will grow as factoring proceeds down the diagonal.

In addition to the number of elements per edge, other factors such as stiff/soft systems (see next section) or poor performance of distorted elements can ill-condition $\underset{\sim}{K}$ and create roundoff error. It is prudent, therefore, to include a roundoff error test in the equation solver, e.g.:

$$\mathcal{C}_D = \text{MAX}[-\log_{10}(D_{mm}/K_{mm})] \quad ; \quad m = 1,2,\ldots,J \tag{26}$$

which directly measures the number of decimal places lost. One should also keep in mind that all factoring and related algorithms (e.g. eigenvalue solvers) are subject to the roundoff effect.

Stiff/soft systems

Finite element models of stiff/soft systems can produce meaningless results if the model consists of small-displacement-theory elements. A stiff/soft system consists of two or more components with significantly different elastic moduli. Systems in which the flexibility of the soft component allows large rigid-body motions of the stiff component are the difficult ones to model. Results can be difficult to evaluate because the solution for one load case can be correct while another can look right but be wrong.

Figure 14 illustrates a case involving the design of a 150-KeV X-ray telescope for flight on a spacecraft. The system consists of two detectors surrounded by a structural box independently mounted on elastomer pads which damp out launch vibrations and squib shocks. Collimators (not shown) cover the box openings to directionally tune the detectors to X-ray sources perpendicular to the page. The box is fabricated from slabs of single-crystal cesium iodide (CsI) doped to scintillate at X-ray energies in the detection band. Scintillations in the box trigger photomultiplier tubes to null out any uncollimated counts. The stiff/soft structural system consists of the CsI box ($E \cong 5\text{x}10^5$ psi) and the elastomer mounts ($E \cong 100$ psi).

The telescope designer requested a finite element analysis of the corner detail to see if the operational stresses would exceed the strength of CsI (about 240 psi). Both launch acceleration loads and differential thermal expansion in orbit had to be considered. Part of the box containing one corner detail was isolated and equilibrating boundary conditions were applied as shown in Figure 15. The model consisted of small-displacement plane continuum elements.

The thermal expansion case was analyzed first, and the model was accepted when the computed nominal thermal stress in the vertical leg was found to agree with hand calculations. The corner thermal stresses were well below the strength of CsI, but analysis of the acceleration case produced corner tensile stresses of about 350 psi, and it appeared that the box would not be able to survive a launch. Fortunately, a stress contour map of the entire detail was to be prepared to document this result. When elements near the ends of the legs were mapped, stresses of the order of 10^6 psi were discovered! A check of the displacement solutions for both cases revealed what had happened. In the launch case, numerical truncation of the applied loads $H_1, M_1, \ldots, V_2$ created a slight moment imbalance on the model. This imbalance was enough to deflect the soft mount, however, in a way that caused the box corner to rotate as a rigid body. At the ends of the legs, the displacements corresponding to this rotation were of the order of the element size, making the small-displacement model invalid.

The launch case was subsequently solved by fixing the nodes at the mount/box interface and ignoring the stress-raising effect of the artificial hard-point thus created. The corrected stresses near the inside corner were well below the strength of CsI. Thus, only a fortuitous decision to map all of the stress data saved an adequate design from rejection based on a meaningless stress analysis.

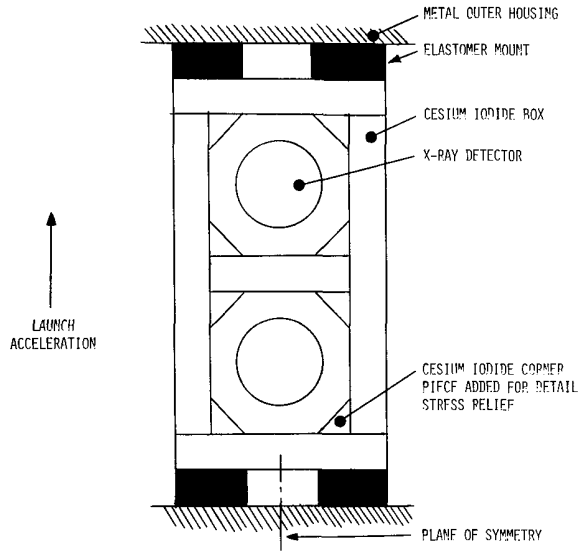

Figure 14. X-ray telescope configuration

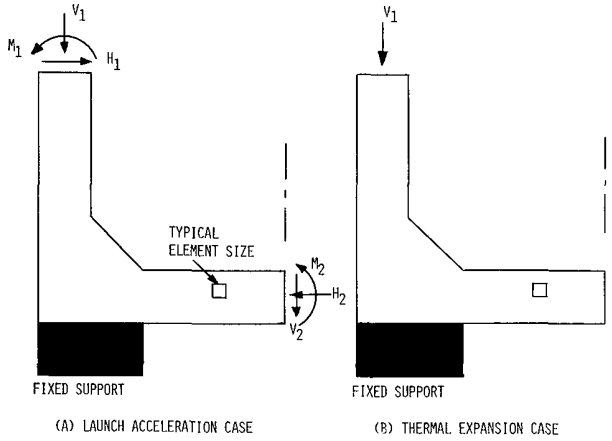

Figure 15. Corner detail finite element model

Counterintuitive behavior

Intuition underlies every structural analysis model. For example, slender beam theory neglects the transverse-shear contribution to beam deflection. This intuition is inaccurate for span/depth ratios less than 10, however, requiring addition of transverse-shear flexibility to the theory to deal with short beams. This limit of slender beam theory is well understood, but analogous subtle effects can cause complex structures to behave counter to the model-maker's intuition, as shown by the following two cases.

In the first case, fracture of a pitch-control crank ring in the propeller of the USS Barbey (DE1088) led to a three-dimensional stress analysis of the failed part. Figure 16 illustrates the location of the failure in the crank-ring/propeller-blade attachment detail and shows a cutaway view of a similar design for the USS Spruance (DD963). The DD963 design was also analyzed to see if Spruance-class crank rings should be expected to have failures similar to the DE1088 fracture.[33]

Figure 17 is a perspective plot of the DE1088 crank ring finite element grid. The model consisted of 4-node tetrahedra and 8-node hexahedra. Typical element sizes were much larger than the scale of the significant stress-raising details and many elements were stretched to the limit of acceptable aspect ratio in order to model the complex crank ring with a reasonable number of nodes. Hence, the model was used only to compute nominal section stresses, and handbook factors for threads or fillets were then applied to translate the nominal values into detail stresses. This procedure was adopted to cope with an obvious limitation of the finite element model.

However, a more subtle aspect of the structure's behavior was not recognized. The loads applied by the propeller blade through its attachment bolts to the crank ring were calculated under the assumption that the bolt preloads made the structural stack behave as an integral unit. In particular, beam-theory distributions were used for applied stresses corresponding to bending moments from the propeller blade. Later Navy tests of strain-gaged propellers showed that the actual bending stresses were concentrated at specific bolts. Lateral prying of the affected bolts due to local flexibilities in the blade palm was found to be the cause (see Figure 18). Thus, the original intuition about integral stack behavior under preload conditions was wrong, and subsequent analyses had to be modified to include nonlinear contact at the blade-palm/crank-ring interface.

In the second case, a finite element analysis was used to correct an intuition based on shell theory. The object of concern was the quartz window in the Čerenkov radiation counter shown in Figure 19. The window was a thick-walled shallow spherical cap designed to withstand the internal pressure in the counter vessel. The original stress analysis was based on a constant-thickness shell theory, and the curvature of the window's edge was also neglected. Under these assumptions, pressure on the convex side always leads to compressive

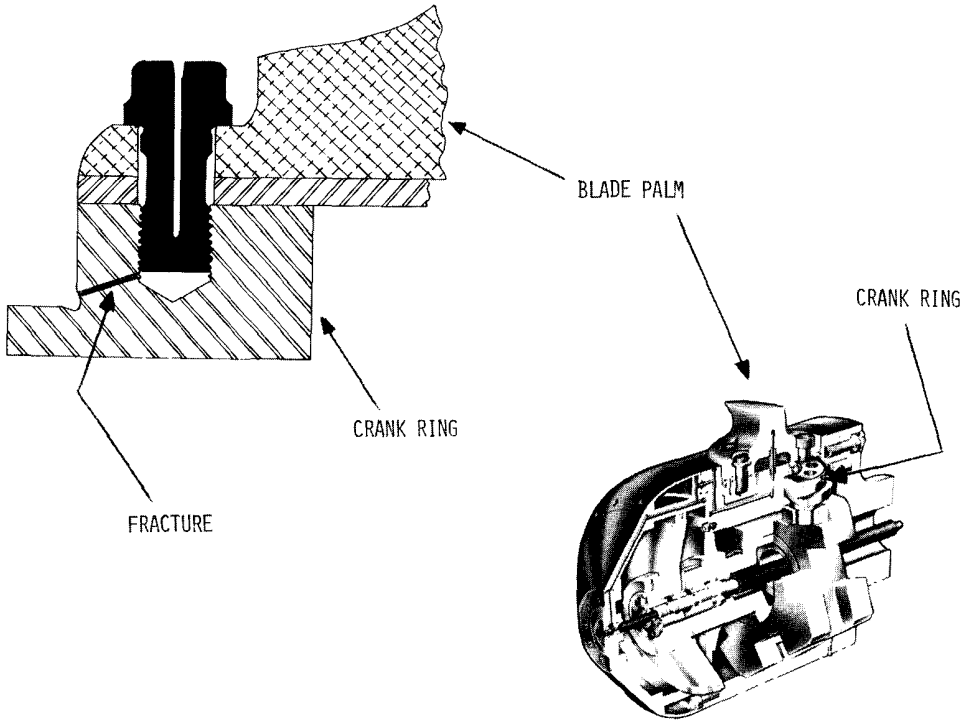

Figure 16. Blade attachment details in controllable-pitch propeller

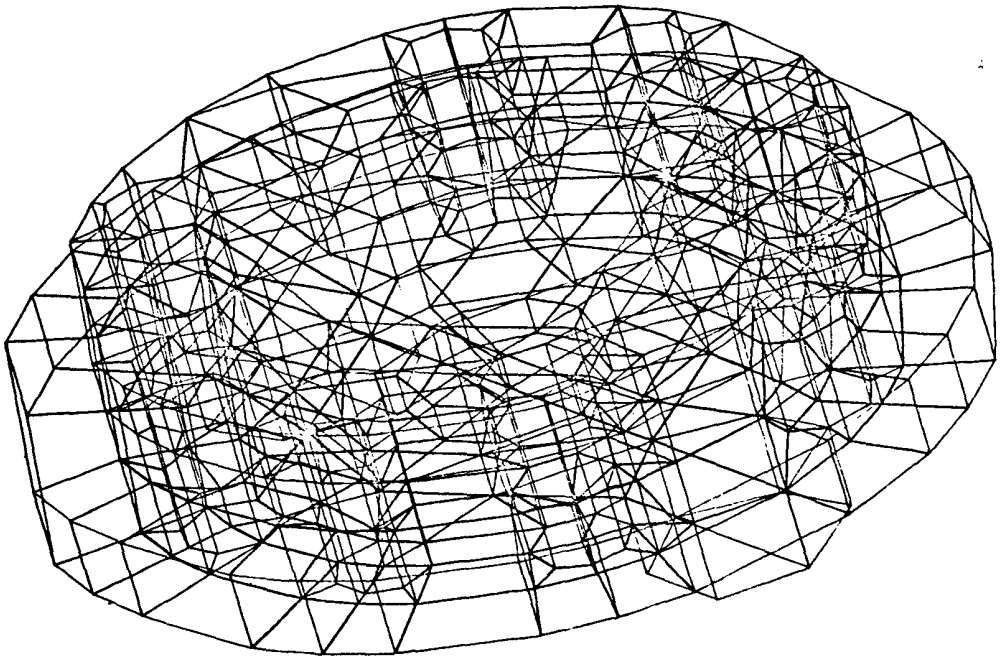

Figure 17. USS Barbey crank ring finite element model

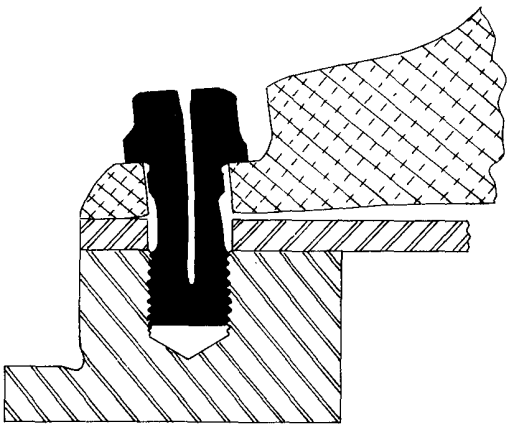

Figure 18. Prying action of blade palm on attachment bolt

stresses in the shell.

The designer was concerned about the possibility of local tensile stresses, however, in view of the strength properties of quartz (about 7 ksi tensile strength as compared to 120 ksi compressive strength). Axisymmetric ring elements were used to model the exact curvatures on all the window boundaries. Figure 20 presents the principal-stress contour plots obtained from the finite element analysis, showing the existence of a tension pocket near the edge of the window. Subsequent development tests showed that the critical pressure and failure location agreed with the finite element predictions.[34]

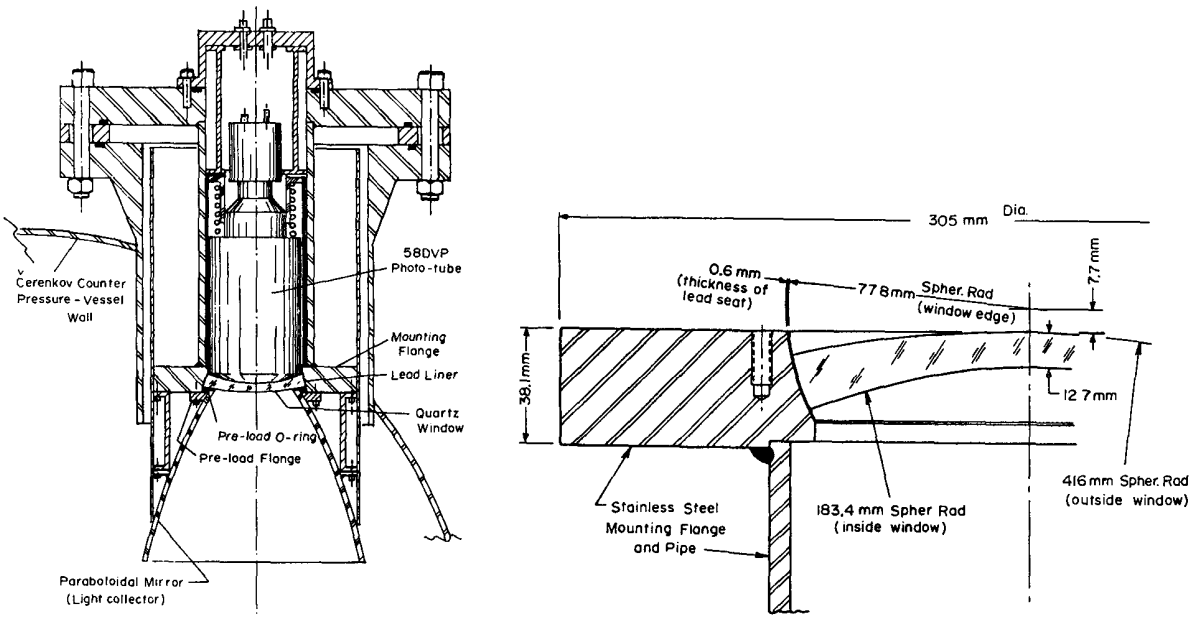

(a) Counter configuration (b) Window detail

Figure 19. Cerenkov radiation counter

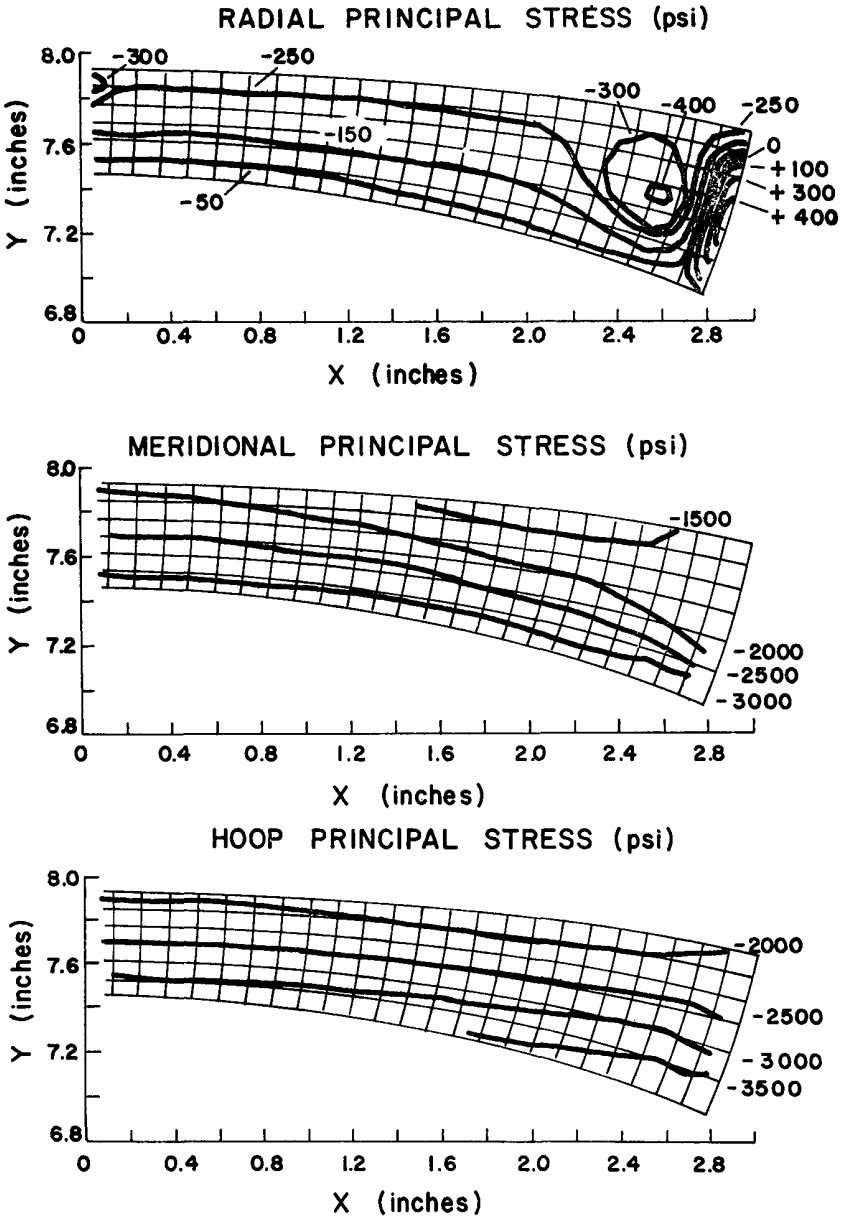

Figure 20. Counter window stresses

Paying attention to significant details

Structural components usually fail at joints, bonds, or geometrical stress-raisers. The finite element analyst must accordingly shift his attention from nominal section stresses, which his models easily produce, to the significant construction details which control the strength of the structure. There are four different ways to shift the focus.

First, it is common practice in plane elasticity to use triangle elements to locally refine a grid near a simple stress-raiser (see Figure 21A). One can also use special-purpose hybrid elements to refine the grid (Figure 21B) or mixed-order isoparametric elements to increase the order of the element polynomials (Figure 21C). Equivalent procedures using tetrahedra and hexahedra are possible for three-dimensional grids. The last two approaches are easier to visualize spatially, but only the tetrahedron solid elements are commonly available in general-purpose programs.

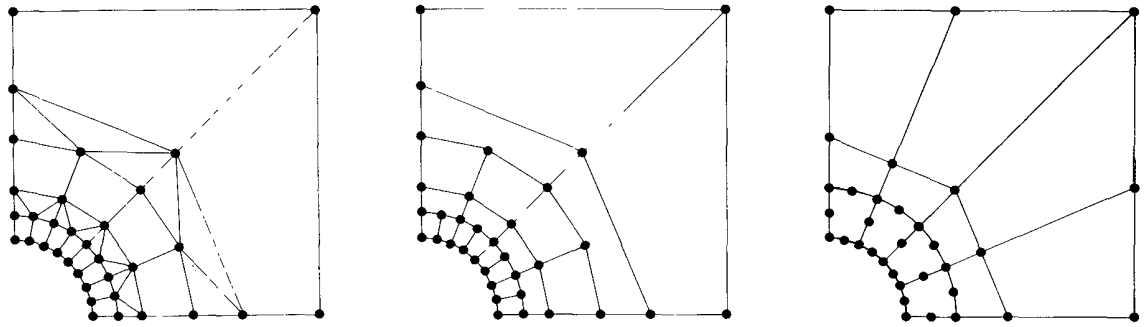

(a) Bilinear quadrilaterals refined by constant-strain triangles

(b) Bilinear quadrilaterals refined by 5-node hybrid pentagon elements (displacement linear between each node pair)

(c) Transition from bilinear to biquadratic quadrilaterals via 5-node mixed-order isoparametric elements

Figure 21. Alternate methods of grid refinement

Second, one can use the substructuring procedure available in some general-purpose programs. A region surrounding the detail is isolated from the model, and the remainder of the model is designated as the substructure. The degrees of freedom in the substructure are then conceptually divided into an interior set (I) and a boundary set (B). The boundary set includes the nodes at which external loads are to be applied and the nodes along the isolation cut. The global stiffness matrix of the substructure,

$$\underset{\sim}{K} = \begin{bmatrix} \underset{\sim}{K}_{BB} & \underset{\sim}{K}_{BI} \\ \underset{\sim}{K}^{T}_{BI} & \underset{\sim}{K}_{II} \end{bmatrix} \tag{27}$$

can be reduced by means of a procedure similar to factoring to the form:

$$\underset{\sim}{K}_{R} = \underset{\sim}{K}_{BB} - (\underset{\sim}{K}_{BI})^{T}(\underset{\sim}{K}_{II})^{-1}(\underset{\sim}{K}_{BI}) \tag{28}$$

and $\underset{\sim}{K}_{R}$ can then be coupled with the isolated region. Substructuring alone offers no benefits in a single analysis, but it can save computing costs in situations involving many cases of different applied loads and/or detail design variations. One should be aware, however, that ill-conditioning of $\underset{\sim}{K}_{II}$ may cause large errors in $\underset{\sim}{K}_{R}$ if the interior set contains a high percentage of the total degrees of freedom in the substructure. Such situations can be corrected by including enough fixed degrees of freedom in the boundary set to suppress all possible rigid-body motions of the substructure.

Third, one can often supplement a general-purpose finite element analysis with handbook formulae or engineering analyses, e.g. as in the ad hoc analysis of the DE1Ø88 crank ring mentioned earlier. Airframe stress analysis is a good example of the application of this approach to design practice. Some aircraft manufacturers combine panel-and-stringer finite element analysis with company-developed procedures for calculating stresses at company-standardized design details. The aircraft industry approach is a sound engineering practice in its environment of evolutionary design work performed by large staffs of junior engineers.

Finally, one can use the hybrid technique to formulate an element which accounts for the stress-raising behavior of a generic detail. Figure 22 illustrates such an element which was specifically developed to wrap around open or bilateral-symmetrically loaded fastener holes by including terms up to cos(2θ) in the angular distribution from the analytical solution for stress near a hole in an infinite plate.[35] The special element couples a coarse exterior grid to an interior grid with refinement comparable to the grid around the C-5A lug (Figure 4). Figure 23 illustrates some results obtained from a program which combined the special element, a hybrid singularity element, and some substructuring to compute stress intensity factors for skin panels with cracked fastener holes.[23] The computations required about one CPU minute per case on an IBM S-370/168.

Modelling complex structures

One must always sacrifice detail to analyze a complex structure. Otherwise the model may exceed the available computing capacity or it may contain an extreme range of element sizes,

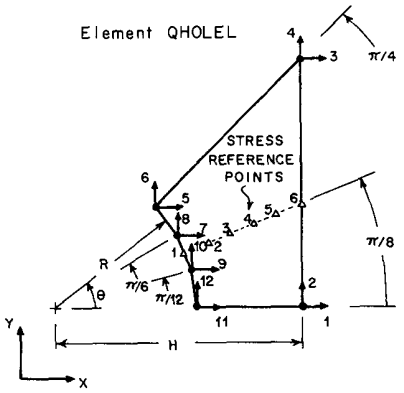

Figure 22. Special-purpose hybrid element for fastener-hole details

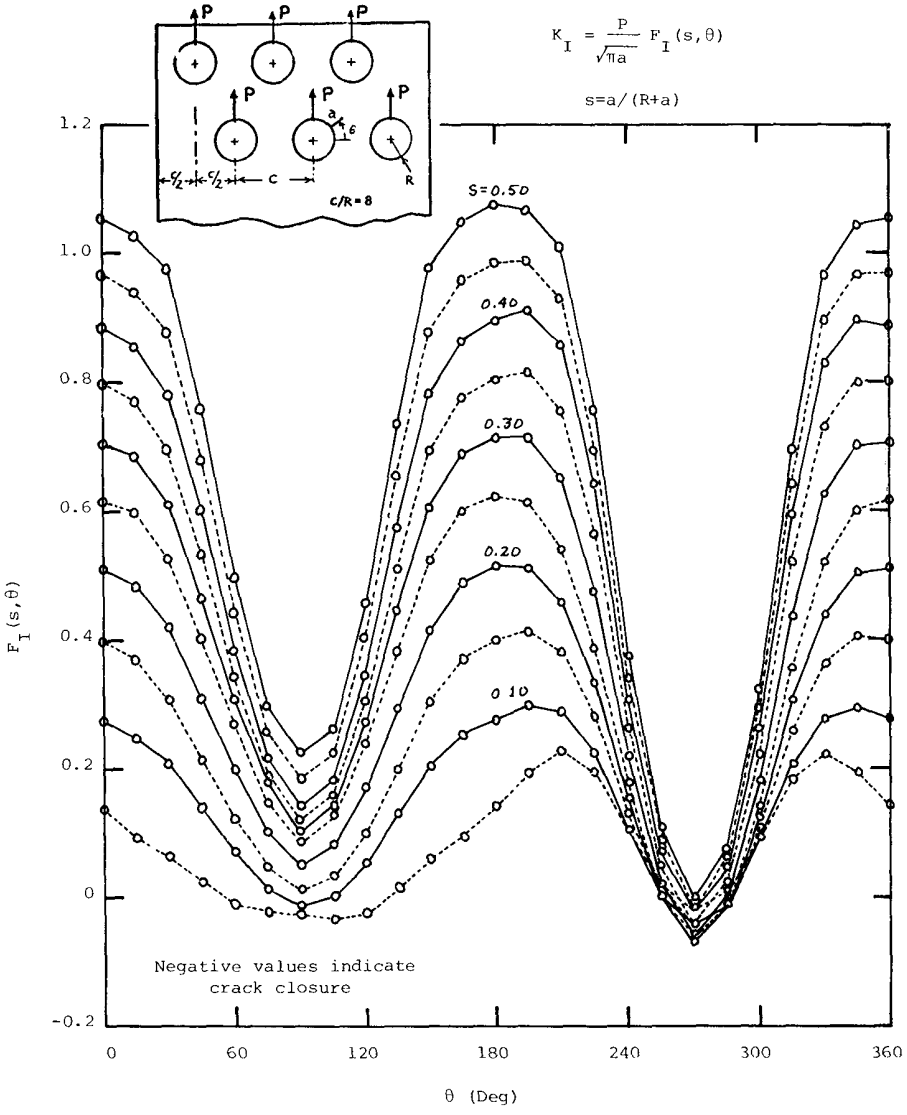

Figure 23. Stress intensity factors for cracked fastener hole in wing skin panel

making it a stiff/soft system. Conversely, the model will not be adequate if too much detail is sacrificed. Creating a balanced and well documented model is the crucial step in the analysis.

Frameworks and frame/plate combinations are generally the most difficult structures to model. For example, consider the A-frame and engine cradle in a recently built fleet of city buses (Figure 24). Early service cracking in these components, particularly the A-frame (Figure 25) led to retrofit-kit modifications. The modified engine cradle (Figure 26) is a good example of structural detail in a frame/plate combination.

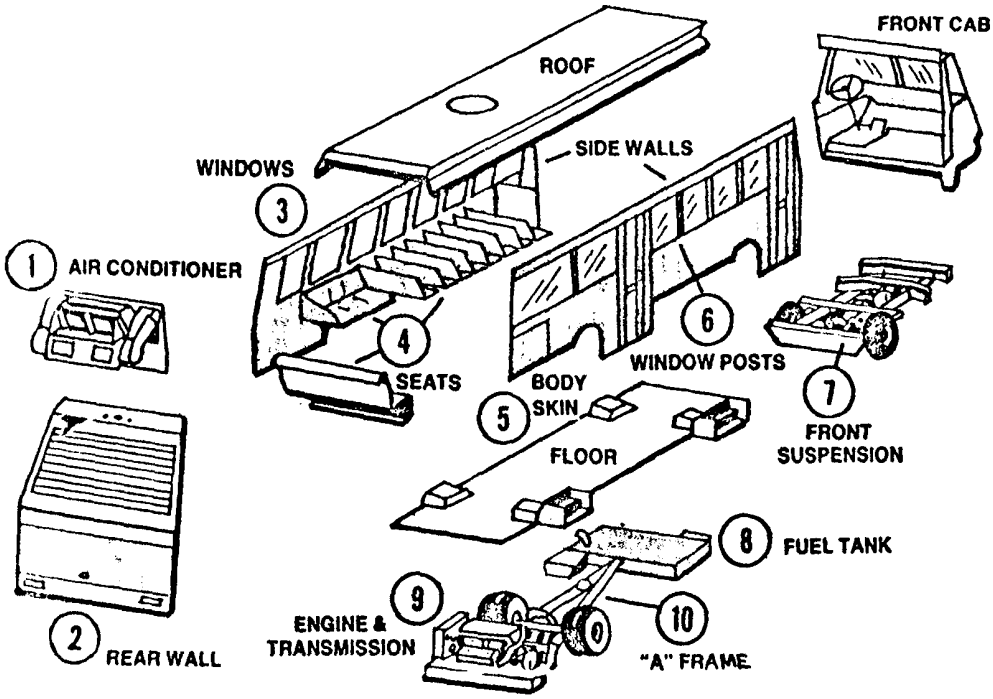

Figure 24. City bus structural configuration

Since either A-frame or engine cradle failures could create potentially unsafe operating conditions, both components had to be analyzed to assess the structural integrity of the modifications.[36] In this case detail could be discarded immediately in areas with low stress (based on strain-gage data) and where original cradles on high-mileage buses had not experienced cracking. However, such shortcuts cannot be taken in pre-production design stress analysis.

In either case the analyst must develop his model by translating production drawings into finite element language. Production drawings focus on locations of and relationships between attachments to guide machinists and welders, i.e. it is up to the analyst to properly locate and orient midplanes and neutral axes. Accurate reconstruction is essential to avoid angular or offset artifacts between adjoining elements. Jointwork often involves physical offsets, however, and the analyst must make auxiliary calculations to reasonably represent true inter-component flexibilities with idealized connector elements. Service loads are usually applied to the structure through complex attachments to finite regions, requiring auxiliary equilibrium analyses to guide the location of loaded nodes.

The foregoing practical factors are further complicated by the need to analyze multiple versions of the component. Structural integrity assessment requires analysis of the original as well as the modified component to assure that predicted lifetimes agree with the observed lifetimes in the original fleet. Pre-production design analysis must keep track of an evolving component. In either case good practice requires that the model evolution be regulated by an updated master schematic supplemented by records of each auxiliary analysis.

Ad hoc schematics were used to control the A-frame and engine cradle finite element models for the bus structural integrity assessment. Figure 27 illustrates the engine cradle schematic. These documents were supplemented by 12 reports of auxiliary analysis pertaining to the models themselves, 26 reports of dynamic analyses performed to characterize the locations and magnitudes of service loads, and 19 reports of detail fatigue analysis based on the finite element model results.

Formalized systems are better than ad hoc procedures for the analysis of pre-production designs if the structure is not one of a kind. For example, some aircraft manufacturers use the finite element model of an airframe as its own master schematic, with CRT and hardcopy display modes for interaction and record-keeping. Many of the supplementary records are also systematized; for example, detail stress and fatigue analyses must be recorded on stress-check forms which guide the junior engineer to correctly combine outputs from the airframe model with the company's handbook procedures for analyzing generic details.

(a) Bus with failed A-frame leg

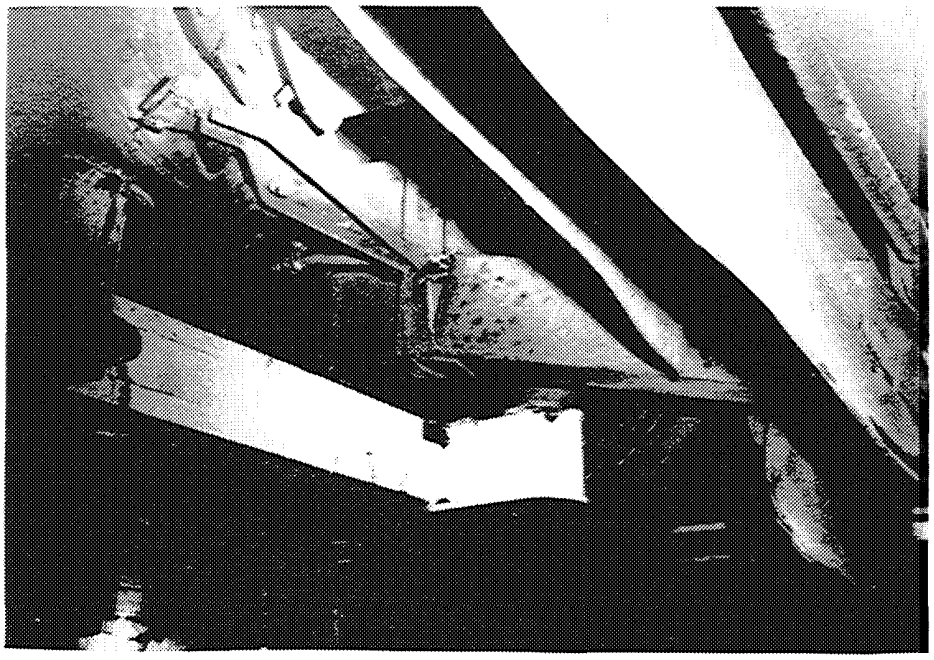

(b) View of failure from below

Figure 25. Example of service failure in rear suspension structure

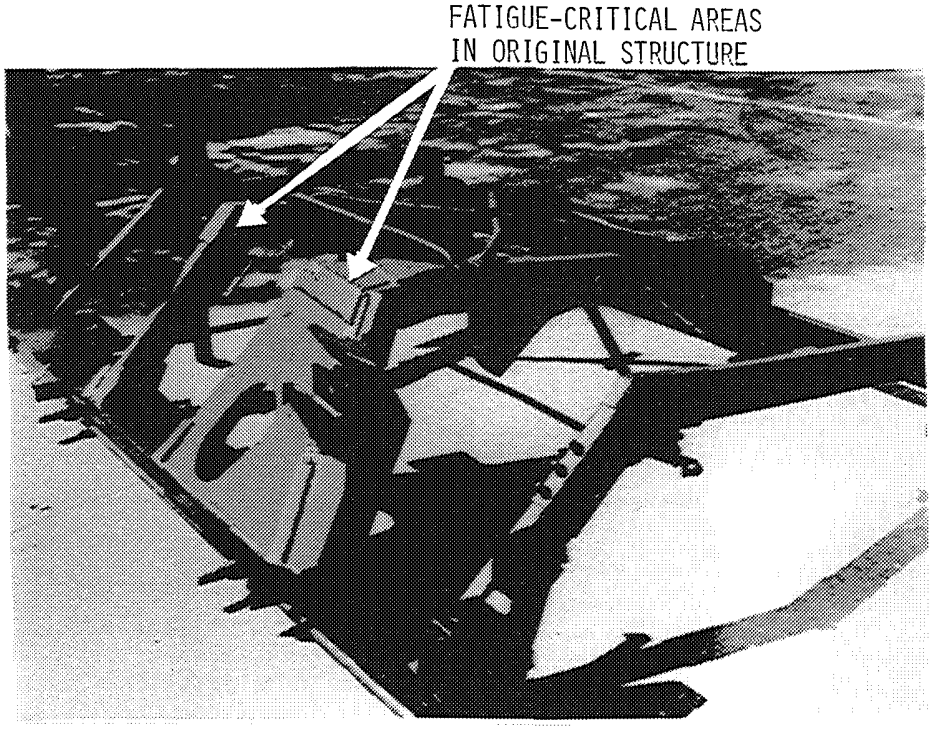

Figure 26. Modified engine cradle structure

Evolving a finite element model of a complex structure involves many people. The opportunities for misunderstanding are numerous, and errors can go undetected if the evolution process is sloppy. The purpose of either ad hoc or formalized procedures for controlling the model is to provide a record which the supervisor can use to detect and correct errors, as well as to interpret results in the light of the model's limitations.

Dynamic analysis

The analyst must calculate the dynamic response of a structure to assess its ability to maintain clearance (e.g. a spacecraft inside its shroud during launch) or to estimate its fatigue safety margin. Hamilton's principle[9] can be used to extend the global equations $\underset{\sim}{\underset{\sim}{K}}\underset{\sim}{q} = \underset{\sim}{Q}$ of static finite element analysis to the dynamic case:

$$\underset{\sim}{\underset{\sim}{M}}\ddot{\underset{\sim}{q}} + \underset{\sim}{\underset{\sim}{C}}\dot{\underset{\sim}{q}} + \underset{\sim}{\underset{\sim}{K}}\underset{\sim}{q} = \underset{\sim}{Q} \tag{29}$$

where the nodal displacements $\underset{\sim}{q}$ and loads $\underset{\sim}{Q}$ are time-dependent, and where $\underset{\sim}{\underset{\sim}{M}}$ and $\underset{\sim}{\underset{\sim}{C}}$ are symmetric mass and damping matrices, respectively, with $\underset{\sim}{\underset{\sim}{M}}$ positive-definite (i.e. $\underset{\sim}{\underset{\sim}{M}}^{-1}$ exists). The following subsections briefly sketch the practical application of numerical methods to dynamic analysis. The discussion is restricted to linear systems except where noted otherwise.

Determination of natural frequencies

Since most structures are lightly damped, it is customary to begin a dynamic analysis by computing the undamped natural frequencies and mode shapes. Accordingly, $\underset{\sim}{\underset{\sim}{C}}$ and $\underset{\sim}{Q}$ are set equal to zero, and Eq. 29 reduces to the eigenproblem:

$$\underset{\sim}{\underset{\sim}{K}}\underset{\sim}{\underset{\sim}{U}} = \underset{\sim}{\underset{\sim}{M}}\underset{\sim}{\underset{\sim}{U}}\left[\omega^2\right] \tag{30}$$

$$\underset{\sim}{\underset{\sim}{U}} = [\underset{\sim}{u}_1\ \underset{\sim}{u}_2\ \cdots\ \underset{\sim}{u}_J] \tag{31}$$

for a J-degree-of-freedom model, where $\underset{\sim}{u}_j$ and ω_j are respectively the nodal-displacement mode shape (eigenvector) and the natural frequency of the jth vibration mode.

The eigensolutions $\underset{\sim}{u}_j, \omega_j$ can be computed in principle by finding the roots of the determinant of Eq. 30:

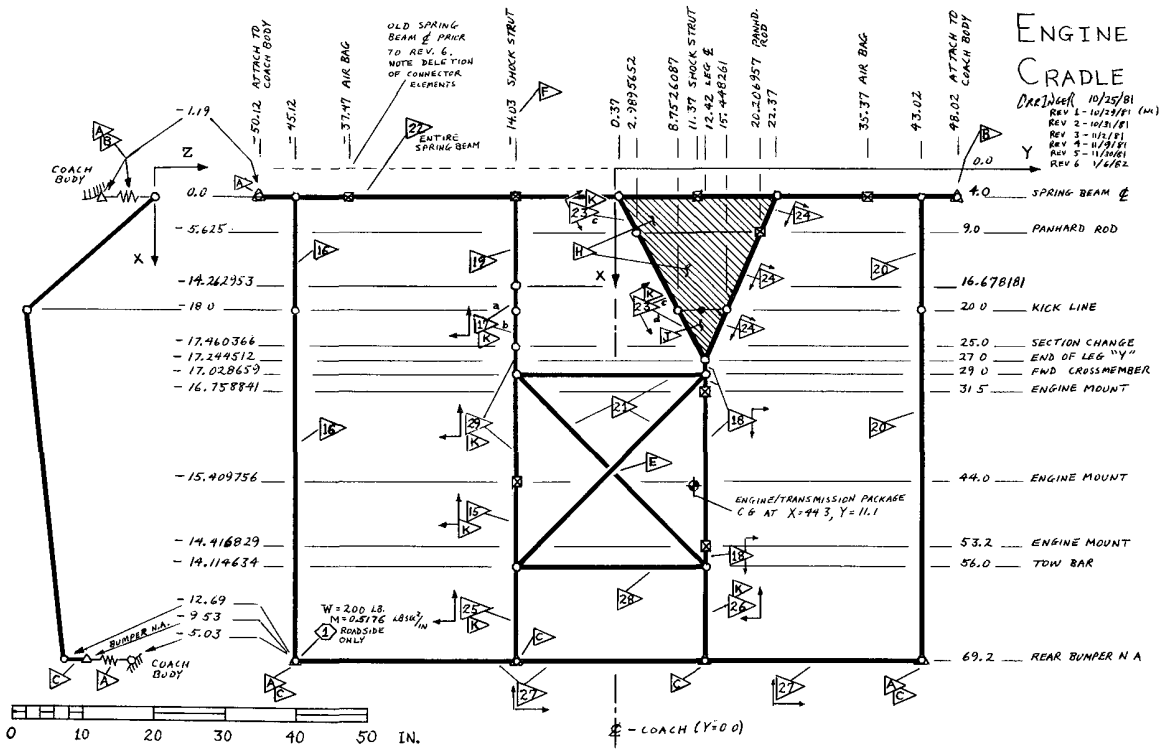

(a) Finite element model schematic

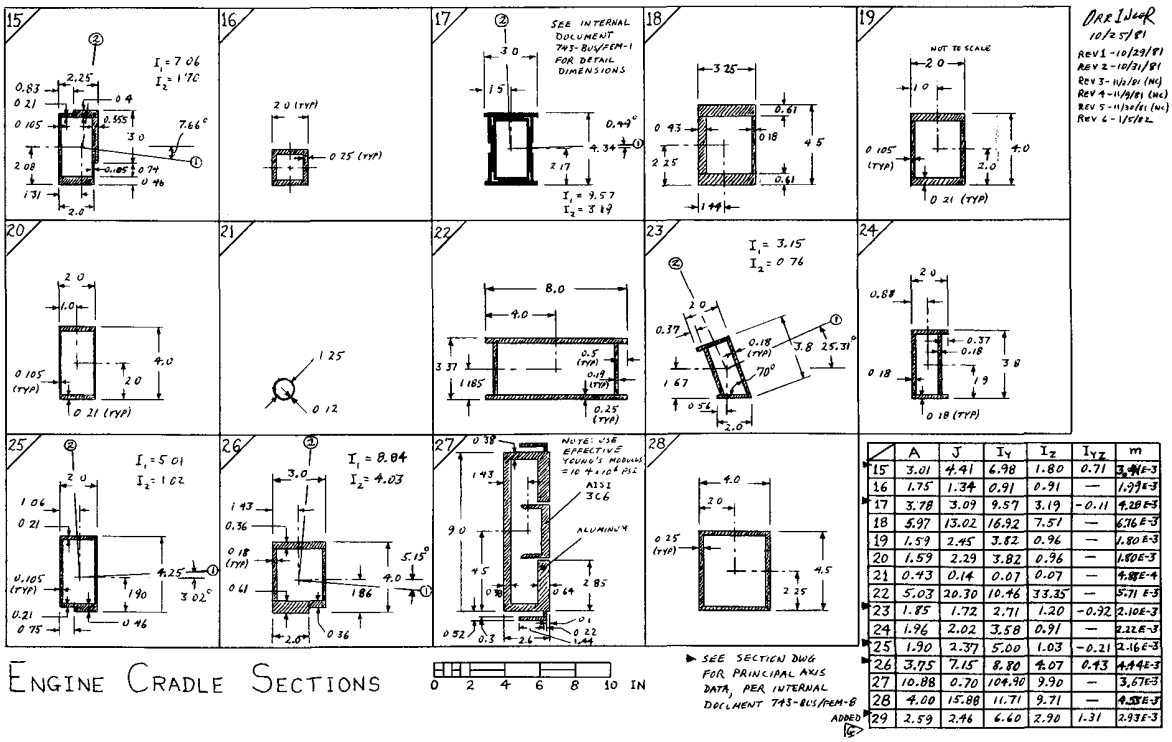

	A	J	I_Y	I_Z	I_{YZ}	m
15	3.01	4.41	6.98	1.80	0.71	3.44E-3
16	1.75	1.34	0.91	0.91	—	1.99E-3
17	3.78	3.09	9.57	3.19	-0.11	4.28E-3
18	5.97	13.02	16.92	7.51	—	6.16E-3
19	1.59	2.45	3.82	0.96	—	1.80E-3
20	1.59	2.29	3.82	0.96	—	1.80E-3
21	0.43	0.14	0.07	0.07	—	9.88E-4
22	5.03	20.30	10.46	33.35	—	5.71 E-3
23	1.85	1.72	2.71	1.20	-0.92	2.10E-3
24	1.96	2.02	3.58	0.91	—	2.22E-3
25	1.90	2.37	5.00	1.03	-0.21	2.16E-3
26	3.75	7.15	8.80	4.07	0.43	4.44E-3
27	10.88	0.70	104.90	9.90	—	3.67E-3
28	4.00	15.88	11.71	9.71	—	4.55E-3
29	2.59	2.46	6.60	2.90	1.31	2.93E-3

(b) Structural section details

Figure 27. Ad hoc documentation of engine cradle finite element model

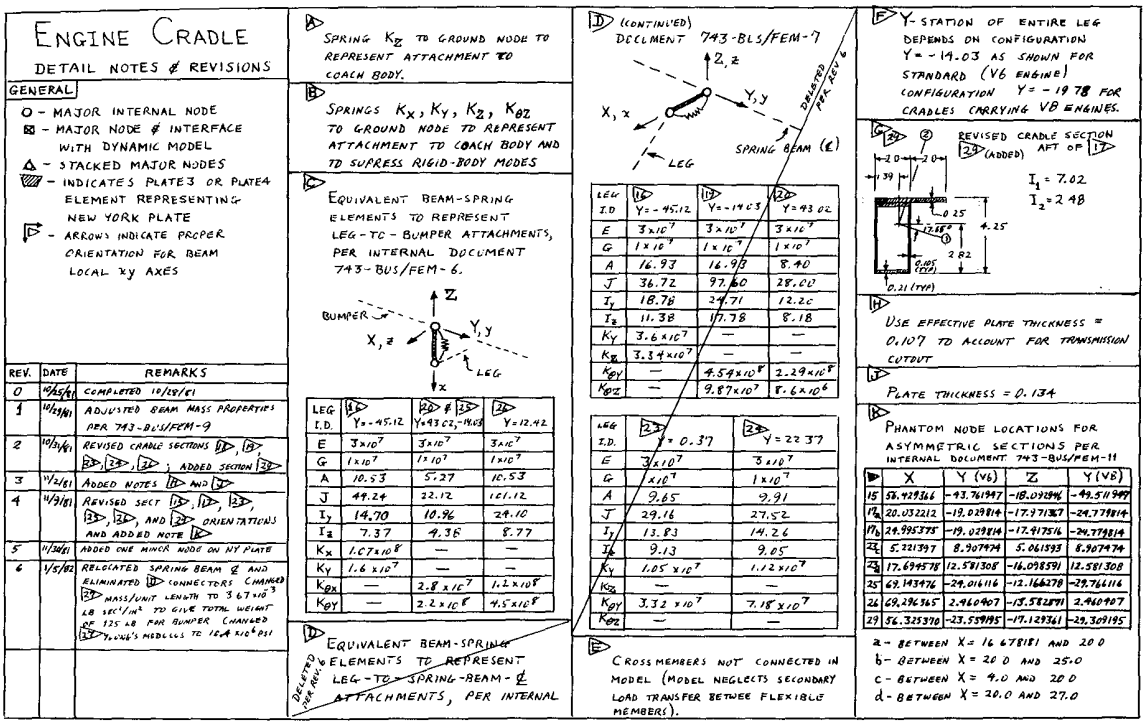

(c) Model evolution notes

Figure 27 (concluded)

$$\left| \underset{\sim}{K} - \omega^2 \underset{\sim}{M} \right| = 0 \tag{32}$$

This procedure is impractical in general when J > 4, however, and a two-step matrix iteration:

$$\underset{\sim}{A}\underset{\sim}{Z} = \underset{\sim}{Z}[\lambda] \quad ; \ \underset{\sim}{A} \text{ symmetric; } \underset{\sim}{Z} = [\underset{\sim}{z}_1 \ \underset{\sim}{z}_2 \ \cdots \ \underset{\sim}{z}_J] \tag{33}$$

is actually used to solve the problem. In the first step $\underset{\sim}{A} = \underset{\sim}{M}$, and in the second step:

$$\underset{\sim}{A} = \underset{\sim}{M}^{-1/2}\underset{\sim}{K}\underset{\sim}{M}^{-1/2} \ ; \ [\lambda] = [\omega^2] \tag{34}$$

Note that $\underset{\sim}{Z}^{-1} = \underset{\sim}{Z}^T$ is a fundamental property of Eq. 33. It is then easy to show that $\underset{\sim}{M}^{-1/2} = \underset{\sim}{Z}[\lambda^{-1/2}]\underset{\sim}{Z}^T$ and hence $\underset{\sim}{M}^{-1/2}\underset{\sim}{K}\underset{\sim}{M}^{-1/2}$ is symmetric. Also, the eigenvectors are computed from $\underset{\sim}{U} = \underset{\sim}{M}^{-1/2}\underset{\sim}{Z}$ after the second iteration.

Plane rotation matrices $\underset{\sim}{R}$ are used to iterate the matrix $\underset{\sim}{A}$ such that $\underset{\sim}{R}^T\underset{\sim}{A}\underset{\sim}{R}$ transforms one off-diagonal coefficient A_{ij} to zero:

$$\underset{\sim}{R} = \begin{array}{c} \begin{matrix} & & & & \text{col. i} & & \text{col. j} & & \end{matrix} \\ \begin{bmatrix} 1 & 0 & 0 & \cdots & 0 & \cdots & 0 & \cdots \\ 0 & 1 & 0 & \cdots & 0 & \cdots & 0 & \cdots \\ \vdots & & \ddots & & \vdots & & \vdots & \\ & & & & \cos\theta & \cdots & -\sin\theta & \\ & & & & \vdots & & \vdots & \\ & & & & \sin\theta & \cdots & \cos\theta & \\ & & & & & & & \ddots \end{bmatrix} \end{array} \begin{matrix} \\ \\ \\ \text{row i} \\ \\ \text{row j} \\ \\ \end{matrix} \tag{35}$$

$$2\theta = \tan^{-1}[A_{ij}/(A_{ii}-A_{jj})] \tag{36}$$

Roundoff errors can occur when the eigenvalues cluster ($A_{ii} \approx A_{jj}$) and will affect any parallel-solution algorithm.

If successive rotations $\underset{\sim}{R}_1$, $\underset{\sim}{R}_2$, ... are used to sweep out the off-diagonal terms, the transformed matrix $\underset{\sim}{A}$ and the product $\underset{\sim}{R}_1\underset{\sim}{R}_2\ldots$ tend toward $[\lambda]$ and $\underset{\sim}{Z}$, respectively. These asymptotes cannot be reached in a finite number of steps because each rotation undoes some of the work of the earlier rotations. The process is convergent, however, and the off-diagonal terms can be swept repeatedly until the quantity:

$$[\sum(A_{ij})^2/\sum(A_{ii})^2]$$

decreases to a specified tolerance. This algorithm is known as Jacobi iteration and is useful up to about J = 50.

Many other schemes are available for larger systems.[37,38] For example, the modified QR method found in some of the older general-purpose finite element programs is most efficient when all J natural frequencies are sought from a J-degree-of-freedom model. The QR algorithm reduces $\underset{\sim}{A}$ to tridiagonal form in a finite number of plane rotations:

$$\underset{\sim}{A} = \begin{bmatrix} A_{11} & & & & \text{(Symmetric)} \\ A_{12} & A_{22} & & & \\ 0 & A_{23} & A_{33} & & \\ 0 & 0 & A_{34} & A_{44} & \\ \cdot & \cdot & \cdot & \cdot & \cdot \end{bmatrix} \tag{37}$$

The determinant $|\underset{\sim}{A} - \lambda\underset{\sim}{I}|$ can now be rapidly computed from the following recursion formulae:

$$\begin{aligned} P_0(\lambda) &= 1 \\ P_1(\lambda) &= A_{11} - \lambda \\ P_j(\lambda) &= (A_{jj} - \lambda)P_{j-1} - (A_{j-1,j})^2 P_{j-2} \quad ; \; j = 2,3,\ldots,J \end{aligned} \tag{38}$$

Equations 38 are then iterated with trial values of λ, taking advantage of the property that the number of consecutive agreements in sign of P_0, P_1, ... equals the number of roots greater than λ.[39] After the roots have been found and arranged in ascending order, the eigenvectors can be computed from the iteration:

$$\underset{\sim}{z}_j(n+1) = [\underset{\sim}{A}\underset{\sim}{z}_j(n) - \sum_{i=1}^{j-1} \lambda_i \underset{\sim}{z}_i \underset{\sim}{z}_i^T]/\lambda_j \tag{39}$$

where $\underset{\sim}{A}$ is the original matrix. Step 1 ($\underset{\sim}{A} = \underset{\sim}{M}$) requires the eigenvectors to get to step 2 of the structural dynamic problem; the physical eigenvectors $\underset{\sim}{Z} = \underset{\sim}{U}$ may be optionally computed at the end of step 2.

In practice one rarely seeks all J modes because the model does not accurately represent the higher modes and because the higher natural frequencies are generally well above the maximum expected excitation frequency. In this case subspace iteration[40] is the most efficient approach. This algorithm iterates a subset of eigenvectors:

$$\underset{\sim}{U}(n) = [\underset{\sim}{u}_1(n) \; \underset{\sim}{u}_2(n) \; \ldots \; \underset{\sim}{u}_j(n)] \quad ; \; j \ll J \tag{40}$$

used to deflate $\underset{\sim}{K}$ and $\underset{\sim}{M}$ to jXj matrices $\underset{\sim}{k}$ and $\underset{\sim}{m}$, after which the subspace eigenproblem $\underset{\sim}{k}\underset{\sim}{v} = \underset{\sim}{m}\underset{\sim}{v}[\lambda(n)]$ is solved and $\underset{\sim}{U}$ is updated:

$$\underset{\sim}{k} = \underset{\sim}{U}^T(n)\underset{\sim}{K}\underset{\sim}{U}(n) \quad ; \quad \underset{\sim}{m} = \underset{\sim}{U}^T(n)\underset{\sim}{M}\underset{\sim}{U}(n) \tag{41}$$

$$\underset{\sim}{U}(n+1) = \underset{\sim}{K}^{-1}\underset{\sim}{M}\underset{\sim}{U}(n)\underset{\sim}{v} \tag{42}*$$

The procedure rapidly converges $\underset{\sim}{U}(n)$ and $[\lambda(n)]$ to the j lowest-frequency modes. The subspace iteration method is found in many of the newer general-purpose finite element

*A static equation-solver (e.g. triple factoring) is actually used in lieu of computing $\underset{\sim}{K}^{-1}$. For unrestrained structures ($\underset{\sim}{K}$ singular), the original problem must be modified to $(\underset{\sim}{K} + \phi\underset{\sim}{M})\underset{\sim}{U} = \underset{\sim}{M}\underset{\sim}{U}[\lambda + \phi]$ ($\phi > 0$) to permit factoring.

programs.

The natural frequencies of highly damped structures can be determined by retaining the $\dot{q}$ term in Eq. 29, but the eigenvalues are complex numbers and the numerical procedures consume much more computing time.[37,38] The matrix iterations for either complex or real eigenvalues should be performed in double precision to avoid serious roundoff errors.[37]

Element mass matrices

The global mass matrix M is assembled from element mass matrices m. An element can have either a lumped or a "consistent" mass matrix.

A lumped mass matrix is defined by rational division of the element's mass into diagonal values for each node, e.g.:

$$m = (\rho At/4)I \tag{43}$$

for a bilinear-displacement plane-stress rectangle of mass density ρ, area A, and thickness t. Rational lumping for elements with arbitrary shapes and/or higher-order interpolations is difficult and non-unique.[41]

For assumed-displacement elements in which the internal displacement field u is related to the nodal displacements q by $u = Bq$, a consistent mass matrix can be computed from the interpolation functions B:

$$m = \int_V \rho B^T B dV \tag{44}$$

where V is the element's volume. For hybrid elements, in which u is generally defined only on the boundaries for the purpose of stiffness matrix formation, one can define a "hybrid-consistent" mass matrix by extrapolating B into the element's volume and using Eq. 44. Consistent mass matrices generally have off-diagonal terms, but they avoid the difficulties of lumping and are particularly convenient for dealing with the rotary inertias required by beam and plate bending elements.

Whether a lumped or consistent mass matrix gives the better answer depends on the element performance characteristics. This can be seen by examining the Rayleigh quotient[9] for an approximate frequency in terms of an assumed global mode shape u:

$$\omega^2 \cong (u^T K u)/(u^T M u) \tag{45}$$

A diagonal mass matrix maximizes the denominator in Eq. 45. Hence, lumped masses should be used to correct the tendency of conformal elements to be over-stiff ($u^T K u$ too large), but consistent masses give better results with nonconformal elements.

Response equations for lightly damped structures

The dynamical equations of a lightly damped structure can be simplified by transforming them from the nodal displacements q to the modal coordinates $\bar{q}$:

$$q = U\bar{q} \tag{46}$$

where U are the eigenvectors and $\bar{q}(t)$ are the time-dependent spatial amplitudes of the natural modes. Substitution of Eq. 46 in Hamilton's principle reduces Eq. 29 to:

$$[\bar{M}]\ddot{\bar{q}} + \bar{C}\dot{\bar{q}} + [\bar{K}]\bar{q} = \bar{Q} \tag{47}$$

where

$$\begin{aligned} [\bar{M}] &= U^T M U \quad ; \quad \bar{C} = U^T C U \\ [\bar{K}] &= U^T K U \quad ; \quad \bar{Q} = U^T Q \end{aligned} \tag{48}$$

Note that while $[\bar{K}]$ and $[\bar{M}]$ are always diagonal, $\bar{C}$ will not be diagonal unless C happens to be a linear combination of K and M. It is obviously advantageous to have $\bar{C}$ diagonal so that the modal equations are completely uncoupled. There are two practical approaches to decoupling.

The more common approach is to sidestep the issue of element damping by assigning modal damping factors directly. The matrix $\bar{C}$ is implicitly assumed to be diagonal, and Eq. 47 is recast in the nondimensional form:

$$\ddot{\bar{q}} + [2\zeta\omega]\dot{\bar{q}} + [\omega^2]\bar{q} = [\bar{M}^{-1}]\bar{Q} \tag{49}$$

where $\zeta_j = C_j/2\sqrt{K_j M_j}$ is the damping factor for the jth mode. One can justify this approach by noting that joint friction and air drag rather than structural continuum properties are the primary sources of damping, i.e. element damping matrices which might lead to a nondiagonal $\underset{\sim}{C}$ have little meaning.

Modal damping factors are convenient to use, but their selection requires good judgement based on knowledge of the dynamic behavior of real structures. For example, inexperienced analysts sometimes make the mistake of computing large-amplitude service motions based on damping factors measured in small-amplitude vibration tests. The true situation is that joint friction is a much more effective damping mechanism at the larger amplitudes, and the damping factors should be increased accordingly.

The alternate approach is to deal directly with element damping when the structure is a mechanical system containing discrete dampers whose properties are specified. In this case it is unlikely that $\underset{\sim}{C}$ will be a linear combination of $\underset{\sim}{K}$ and $\underset{\sim}{M}$. However, one can approximate the effects of the discrete dampers by averaging their power dissipation over the system's natural modes, e.g.:

$$\underset{\sim}{C}_{AVG} = \eta \underset{\sim}{K} \tag{50}$$

where

$$\eta = (1/J)\sum_{j=1}^{J} (\underset{\sim}{u}_j^T \underset{\sim}{C} \underset{\sim}{u}_j)/(\underset{\sim}{u}_j^T \underset{\sim}{K} \underset{\sim}{u}_j) \tag{51}$$

Equations 50 and 51 are not unique, i.e. combinations of $\underset{\sim}{K}$ and $\underset{\sim}{M}$ can be used, the average can be weighted, and it may be better to average over only a few modes. The averaging procedure should be cautiously applied and correlated with vibration test data.

Response calculations

It is most convenient to use the uncoupled modal equations for computing dynamic responses, but the final answers must be transformed back to physical coordinates. The following paragraphs outline three procedures which conform to these requirements and can easily be programmed as post-processors if not already included in one's general-purpose finite element program.

Frequency response functions (FRF) are often of interest, e.g. when designing spacecraft components to meet FRF specifications in a sinusoidal sweep test on a vibration table. In this case the applied loads are in phase,

$$\underset{\sim}{Q}(t) = e^{i\Omega t}\underset{\sim}{Q} \tag{52}$$

where Ω is the excitation frequency, and the steady-state modal coordinate responses are complex functions:

$$\bar{q}_j(i\Omega) = \mathrm{Re}[\bar{q}_j] + i\,\mathrm{Im}[\bar{q}_j]$$

$$\mathrm{Re}[\bar{q}_j] = \frac{[1-(\Omega/\omega_j)^2]/\bar{K}_j}{[1-(\Omega/\omega_j)^2]^2+[2\zeta_j\Omega/\omega_j]^2}\,\underset{\sim}{u}_j^T\underset{\sim}{Q} = H_j(\Omega)\,\underset{\sim}{u}_j^T\underset{\sim}{Q} \tag{53}$$

$$\mathrm{Im}[\bar{q}_j] = \frac{-2\zeta_j\,\Omega/\omega_j\bar{K}_j}{[1-(\Omega/\omega_j)^2]^2+[2\zeta_j\Omega/\omega_j]^2}\,\underset{\sim}{u}_j^T\underset{\sim}{Q}$$

The nodal displacements can be computed by substituting Eqs. 53 into Eq. 46:

$$\mathrm{Re}[\underset{\sim}{q}] = \underset{\sim}{U}\mathrm{Re}[\bar{\underset{\sim}{q}}] \;;\; \mathrm{Im}[\underset{\sim}{q}] = \underset{\sim}{U}\mathrm{Im}[\bar{\underset{\sim}{q}}] \tag{54}$$

Also, if particular element stresses $\underset{\sim}{\sigma} = \underset{\sim}{B}\underset{\sim}{q}$ are wanted, one need only substitute the product $\underset{\sim}{BU}$ for $\underset{\sim}{U}$ in Eqs. 54.

Service loads are often stationary random processes, i.e. their statistics are independent of time even though one cannot directly specify $\underset{\sim}{Q}(t)$.[42] Service loading from a single random source is specified in terms of its autospectral density $S_Q(\Omega)$, which describes the distribution of mean square as a function of frequency. The RMS of $\underset{\sim}{Q}(t)$ is given by:

$$\underset{\sim}{Q}_{RMS} = \underset{\sim}{Q}\sqrt{\int_o^\infty S_Q(\Omega)\,d\Omega} \qquad (\Omega \text{ in units of Hz}) \tag{55}$$

where $\underset{\sim}{Q}$ in Eq. 55 represents the spatial distribution of the loads. The modal coordinate responses are characterized by a complex spectral density matrix $\underset{\sim}{\bar{S}}$. Only the real part of $\underset{\sim}{\bar{S}}$ is needed for RMS computation; the typical term is given by:

$$Re[\bar{S}_{ij}(\Omega)] = H_i(\Omega)H_j(\Omega)S_Q(\Omega)\underset{\sim}{u}_i^T\underset{\sim}{Q}\underset{\sim}{Q}^T\underset{\sim}{u}_j \tag{56}$$

where H is defined in the second of Eqs. 53. The diagonal of the matrix:

$$(\underset{\sim}{q}\underset{\sim}{q}^T)_{MS} = \underset{\sim}{U}\left(\int_o^\infty Re[\underset{\sim}{\bar{S}}(\Omega)]\,d\Omega\right)\underset{\sim}{U}^T \qquad (\Omega \text{ in units of Hz}) \tag{57}$$

contains the mean squares of the nodal displacements, and similarly $(\ddot{\underset{\sim}{q}}\ddot{\underset{\sim}{q}}^T)_{MS}$ can be computed by substituting $\underset{\sim}{B}\underset{\sim}{U}$ for $\underset{\sim}{U}$. If $\underset{\sim}{Q}(t)$ results from two or more random sources, procedures analogous to Eqs. 56 and 57 can be devised by superposition, but one must account for the cross-spectral densities between the sources.[43]

Stresses from transients such as spacecraft deployment, a bus running over a pot hole, or a railroad wheel striking a rail-end gap in jointed track can affect the integrity of a structure. Dynamic finite element models of structures cannot simulate the local stress waves caused by short transients because the models are based on elliptic field equations, while the stress-wave field equations are hyperbolic. However, dynamic finite element models are worthwhile for investigating ringing and the effects of long transients.

Transient response is often computed by applying finite difference operators[38] to the time derivatives in Eq. 29 and integrating numerically. This approach avoids the need for eigensolution and is useful for treating nonlinear systems.[44] However, explicit finite difference operators introduce frequency distortion, artificial damping, and/or instability characteristics which limit the allowable integration time-step size[45,46] Δt to the order of $1/\omega_{MAX}$, where ω_{MAX} is the highest natural frequency in the model. There are implicit operators which are unconditionally stable for linear systems, but these require matrix equation solving at each time step. Hence, large models consume huge amounts of computing time (typically 20 to 50 CPU seconds per second of real time) to produce useful results.

Working with the uncoupled modal equations is a good alternative for lightly damped linear systems. The modal equations can be integrated analytically if the transient loads $\underset{\sim}{Q}(t)$ are interpolated piece-wise. The resulting numerical procedure is free of the finite difference constraints, and Δt is limited only by the need to make a reasonable approximation of $\underset{\sim}{Q}(t)$. For example, let $\underset{\sim}{Q}(t)$ be linearly interpolated between t_{n-1} and t_n:

$$\underset{\sim}{Q}(t) = [(t_n-t)\underset{\sim}{Q}_{n-1} + (t-t_{n-1})\underset{\sim}{Q}_n]/\Delta t_n \tag{58}$$

where $\underset{\sim}{Q}_n = \underset{\sim}{Q}(t_n)$ and in general $\Delta t_n = t_n - t_{n-1}$ can be varied from one step to another. It is then easy to derive the following procedure for computing the response of the jth modal coordinate (omitting the subscript j from Q, q, K, ζ, and ω for brevity):

$$\begin{aligned}\dot{\bar{q}}_n &= X + e^{-\zeta\omega\Delta t_n}\left[\left(\dot{\bar{q}}_{n-1}-X\right)\cos(\omega_D\Delta t_n) + \right.\\ &\left. + (1/\omega_D)\left(\omega^2\bar{Q}_{n-1}/\bar{K}-\omega^2\bar{q}_{n-1}-\zeta\omega\dot{\bar{q}}_{n-1}-\zeta\omega X\right)\sin(\omega_D\Delta t_n)\right]\end{aligned}$$

$$\begin{aligned}\bar{q}_n &= \bar{Q}_{n-1}/\bar{K} + (\Delta t_n - 2\zeta/\omega)X + \\ &+ e^{-\zeta\omega\Delta t_n}\left[\left(\bar{q}_{n-1}+2\zeta X/\omega-\bar{Q}_{n-1}/\bar{K}\right)\cos(\omega_D\Delta t_n) + \right.\\ &\left. + (1/\omega_D)\left(\dot{\bar{q}}_{n-1}+\zeta\omega\bar{q}_{n-1}-(1-2\zeta^2)X-\zeta\omega\bar{Q}_{n-1}/\bar{K}\right)\sin(\omega_D\Delta t_n)\right]\end{aligned} \tag{59}$$

where

$$X = (\bar{Q}_n-\bar{Q}_{n-1})/\bar{K}\Delta t_n \quad ; \quad \omega_D = \omega\sqrt{1-\zeta^2} \tag{60}$$

The initial conditions $\underset{\sim}{q}_o$ and $\dot{\underset{\sim}{q}}_o$ can be expressed in modal coordinates in accordance with:

$$\underset{\sim}{\bar{q}} = [\underset{\sim}{K^{-1}}]\underset{\sim}{U}^T\underset{\sim}{K}\underset{\sim}{q} \tag{61}$$

Pseudo-dynamic analysis

It is occasionally possible to take a shortcut in dynamic analysis if one has some test data and if the first vibration mode is known to dominate a structure's dynamic response. In this case a static analysis will give a reasonable estimate of the spatial distribution of the dynamic deformations if the spatial distributions of the static and dynamic loads are similar; the test data can then be used to calibrate the amplitude. Structures which accept and react major loads in phase at a few discrete locations are good candidates for this shortcut.

The city bus A-frame mentioned earlier[36] was successfully analyzed in this manner. However, the engine cradle dynamic response could not be reliably estimated from static analyses because engine pitch and roll as well as vertical loads caused significant dynamic stresses in the cradle. Figure 28 illustrates the lack of correlation between the dynamic stresses and the static stresses from vertical loading. Static stresses corresponding to unit pitch and roll conditions could be computed, but the difference in pitch/roll and vertical loading frequencies prevented correlation without load phase information.

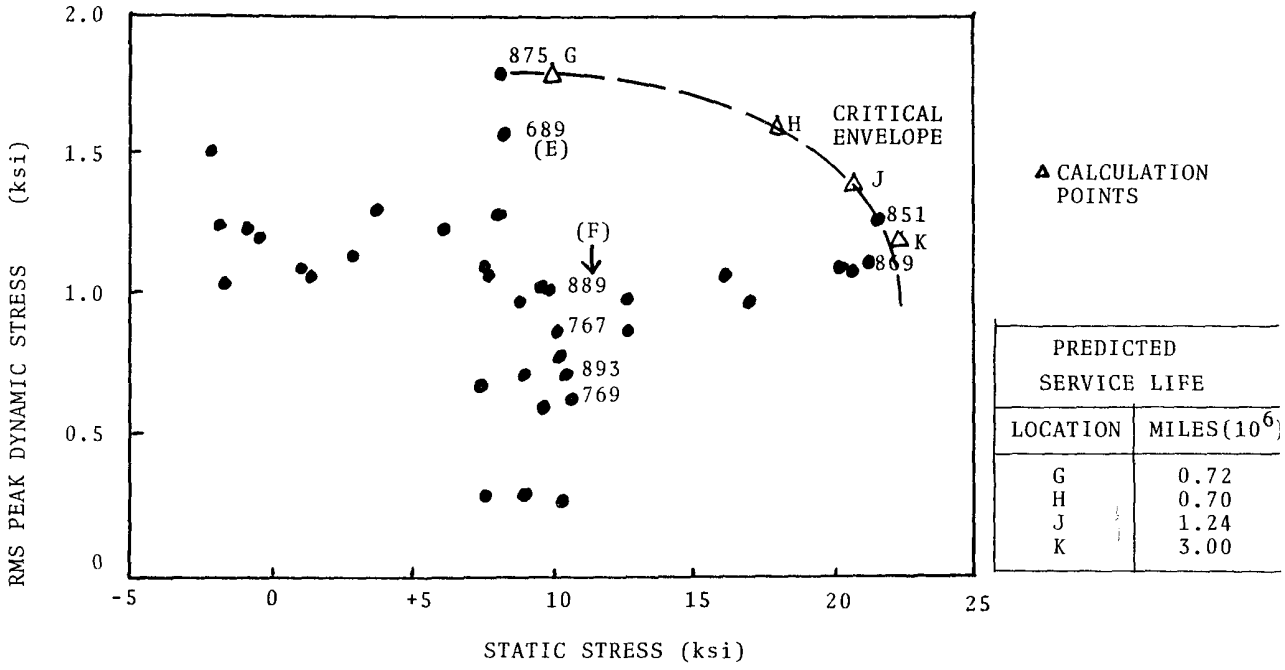

Figure 28. Illustration of lack of correlation between static and dynamic stresses in city bus engine cradle

Stability analysis

Eigensolutions can be used to predict mechanical instabilities as well as natural frequencies by replacing the mass matrix with a stability stiffness matrix. Since the lowest eigenvalue determines the stability boundary, one-mode subspace iteration or simple matrix power iteration should be used in the computation.

For example, the beam element stiffness matrix (see Eq. 20 and Figure 11) was derived from the strain-energy expression:

$$(1/2)\underset{\sim}{q}^T\underset{\sim}{\underset{\sim}{k}}\underset{\sim}{q} = (EI/2)\int_0^{\ell}(d^2w/dx^2)^2dx =$$

$$= (1/2)\underset{\sim}{q}^T\left(EI\int_0^{\ell}(d^2\underset{\sim}{B}^T/dx^2)(d^2\underset{\sim}{B}/dx^2)dx\right)\underset{\sim}{q} \qquad (62)$$

where $w(x) = \underset{\sim}{B}\underset{\sim}{q}$ is a cubic interpolation of the beam deflection. The corresponding stability stiffness matrix is derived from the work done by a column load P moving axially as the beam deflects:

$$P\int_0^{\ell}\left(\sqrt{1+(dw/dx)^2}\ -\ 1\right)dx \cong (P/2)\int_0^{\ell}(dw/dx)^2dx =$$

$$= (1/2)\underset{\sim}{q}^T\left(P\int_0^{\ell}(d\underset{\sim}{B}^T/dx)(d\underset{\sim}{B}/dx)dx\right)\underset{\sim}{q} = (1/2)\underset{\sim}{q}^T(P\underset{\sim}{k}_s)\underset{\sim}{q} \tag{63}$$

$$\underset{\sim}{k}_s = (1/30\ell)\begin{bmatrix} 36 & & (\text{Symmetric}) & \\ -3\ell & 4\ell^2 & & \\ -36 & -3\ell & 36 & \\ 3\ell & -2\ell^2 & -3\ell & 4\ell^2 \end{bmatrix} \tag{64}$$

Equating the strain energy and the external work then leads to the equilibrium condition:

$$\underset{\sim}{k}\underset{\sim}{q} = P\underset{\sim}{k}_s\underset{\sim}{q} \tag{65}$$

for a single-element buckling analysis. The matrices $\underset{\sim}{k}$ and $\underset{\sim}{k}_s$ can also be assembled to create structural stability models,[8] and continuum buckling problems can be similarly investigated with plate elements.[8] The lowest eigenvalue P is the critical buckling load.

Finite element models can also be used to investigate flutter and hunting instabilities. Unsteady aerodynamic forces cause lifting surface flutter and appear in the stability stiffness matrix.[47] Railroad vehicles can experience hunting instability driven by unsteady gravity and creepage forces at the wheel/rail contact points.[48,49] Vehicle speed is the eigenvalue in both cases. The stability stiffness matrices for both flutter and hunting are complex and thus require complex eigensolution algorithms. These problems also differ from buckling in that the stability boundary results from the frequency coalescence of two natural vibration modes, not necessarily the two lowest modes of the structure. Hence, one must retain perhaps 10 modes in the finite element model to estimate the critical speed, and even so there is no guarantee that the two critical modes will have been retained.

Concluding remarks

The examples presented in this paper demonstrate that the finite element method is not a panacea for analyzing complex structures. Both senior engineers responsible for the structure and junior engineers responsible for detail stress analysis must remember that a finite element program is not a substitute for good engineering practice. The method is convenient, however, and is often the best way to get the necessary answers if the following guidelines are kept in mind.

Test new programs and new applications of old programs

Does the software actually do what the user's guide and comment cards say it does?

Avoid theoretical overkill

Tailor the analytical approach to symmetries or near-symmetries of the structure and environment. Concentrate on major behavior (inextensional bending, plane stress, skin/stringer construction, etc.).

Avoid model overkill

Seek the simplest model that will adequately simulate the transfer of applied loads through major components to reaction points. Reserve the finite element method as a last resort for cases where engineering models are inadequate. Limit finite element detail to the level of the other approximations made to create the model (shapes, attachments, knowledge of load distributions, etc.). Does the precision of the model exceed the precision required of the results?

Seek a well conditioned model

The grid pattern should please the eye. Grade gently to fine grids in regions where high stress gradients are expected. Be aware of the performance limits arising from element interpolations and roundoff effects.

Control the model

Document evolution as it occurs. Keep the structure designer in the loop. Is the reasoning behind each revision clearly stated? Does everyone understand and agree on physical interpretation of the results?

Qualify the results

Is the model in equilibrium? Do the displacements and stresses behave reasonably everywhere in the model? Do key results correlate with test data?

Maintain adequate margins

Remember that design margins are determined by the component's function, the structure's mission, and the fabricator's ability to produce construction quality. The fact that a finite element model is used to compute stresses is no excuse for shaving margins.

References

1. R. Courant, "Variational Methods for the Solution of Problems of Equilibrium and Vibrations," Bulletin of the American Mathematical Society, Vol. 49 (January 1943), 1-23.

2. C.S. Desai and J.F. Abel, Introduction to the Finite Element Method, Van Nostrand Reinhold Company, New York, 1970.

3. R.D. Cook, Concepts and Applications of Finite Element Analysis, Wiley, New York, 1974.

4. K.C. Rockey, H.R. Evans, D.W. Griffiths, and D.A. Nethercot, The Finite Element Method: A Basic Introduction, Wiley, New York, 1975.

5. J.S. Przemieniecki, Theory of Matrix Structural Analysis, McGraw-Hill, New York, 1968.

6. O.C. Zienkiewicz, The Finite Element Method in Engineering Science, McGraw-Hill, London, 3rd ed., 1977.

7. G. Strang and G.J. Fix, An Analysis of the Finite Element Method, Prentice-Hall, Englewood Cliffs, NJ, 1973.

8. P. Tong and J.N. Rossettos, Finite Element Method: Basic Technique and Implementation, MIT Press, Cambridge, MA, 1977.

9. K. Washizu, Variational Methods in Elasticity and Plasticity, Pergamon Press, New York, 3rd ed., 1982.

10. R.J. Roark and W.C. Young, Formulas for Stress and Strain, McGraw-Hill, New York, 5th ed., 1975.

11. O. Orringer, S.E. French, P. Tong, and S.T. Mau, "FEABL V3/R1 User's Guide," Aeroelastic and Structures Research Laboratory, MIT, Cambridge, MA, ASRL TR 162-6, October 1973.

12. G.P. Bazeley, Y.K. Cheung, B.M. Irons, and O.C. Zienkiewicz, "Triangular Elements in Plate Bending - Conforming and Nonconforming Solutions," Proc. First Conference on Matrix Methods in Structural Mechanics, USAF Flight Dynamics Laboratory, Wright-Patterson Air Force Base, Ohio, 1965.

13. M.L. Williams, "Stress Singularities Resulting from Various Boundary Conditions in Angular Corners of Plates in Extension," Journal of Applied Mechanics (1952), 526-528.

14. K.Y. Lin and P. Tong, "Singular Finite Elements for the Fracture Analysis of V-Notched Plate," International Journal of Numerical Methods in Engineering, Vol. 15 (1980), 1343-1354.

15. P. Tong and T.H.H. Pian, "On the Convergence of the Finite Element Method for Problems with Singularities," International Journal of Solids and Structures, Vol. 9 (1973), 313-322.

16. P. Tong and T.H.H. Pian, "A Variational Principle and the Convergence of a Finite Element Method in Solving Linear Elastic Problems," International Journal of Solids and Structures, Vol. 3 (1967), 865-879.

17. R.S. Barsoum, "Application of Quadratic Isoparametric Finite Elements to Linear Fracture Mechanics," International Journal of Fracture, Vol. 10 (1974), 603-605.

18. D.M. Parks, "A Stiffness Derivative Finite Element Technique for Determination of Crack Tip Stress Intensity Factors," International Journal of Fracture, Vol. 10 (1974), 487-502.

19. Y. Yamamoto and N. Tokuda, "Stress Intensity Factors in Plate Structures Calculated by the Finite Element Method," Journal of the Society of Naval Architects, Japan, Vol. 130 (1971).

20. P. Tong, T.H.H. Pian and S.J. Lasry, "A Hybrid Element Approach to Crack Problems in Plane Elasticity," International Journal of Numerical Methods in Engineering, Vol. 7 (1973), 297-308.

21. O. Orringer, "Fracture Mechanics Analysis of an Attachment Lug," Aeroelastic and Structures Research Laboratory, MIT, Cambridge, MA, AFFDL-TR-75-51, January 1976.

22. G. Stalk and O. Orringer, "Fracture Mechanics Analysis of Centered and Offset Fastener Holes in Stiffened and Unstiffened Panels Under Uniform Tension," Aeroelastic and Structures Research Laboratory, MIT, Cambridge, MA, AFFDL-TR-75-70, April 1976.

23. O. Orringer and G. Stalk, "Fracture Mechanics Analysis of Single and Double Rows of Fastener Holes Loaded in Bearing," Aeroelastic and Structures Research Laboratory, MIT, Cambridge, MA, AFFDL-TR-75-71, April 1976.

24. T.H.H. Pian, O. Orringer, G. Stalk, and J.W. Mar, "Numerical Computation of Stress Intensity Factors for Aircraft Structural Details by the Finite Element Method," Aeroelastic and Structures Research Laboratory, MIT, Cambridge, MA, AFFDL-TR-76-12, May 1976.

25. O. Orringer, K.Y. Lin, and J.W. Mar, "Application of Finite-Element Analysis to Develop a Bi-Material Crack-Propagation Laboratory Test Specimen," in Case Studies in Fracture Mechanics (T.P. Rich and D.J. Cartwright, ed.), U.S. Army Materials and Mechanics Research Center, Watertown, MA, AMMRC MS 77-5, June 1977.

26. R.L. Spilker, S.C. Chou, and O. Orringer, "Alternate Hybrid-Stress Elements for Analysis of Multilayer Composite Plates," Journal of Composite Materials, Vol. 11 No. 1 (January 1977), 51-70.

27. A.H. Puppo and H.A. Evensen, "Interlaminar Shear in Laminated Composites Under Generalized Plane Stress," Journal of Composite Materials, Vol. 4 (1970), 204.

28. R.B. Pipes and N.J. Pagano, "Interlaminar Stresses in Composite Laminates Under Uniform Axial Extension," Journal of Composite Materials, Vol. 4 (1970), 538.

29. A. Harris and O. Orringer, "Investigation of Angle-Ply Delamination Specimen for Interlaminar Strength Test," Journal of Composite Materials, Vol. 12 (July 1978), 285-299.

30. C.C. Mei and H.S. Chen, "Hybrid Element for Water Waves," Proc. ASCE Symposium on Modelling Techniques, San Francisco, CA, September 1975.

31. P. Tong, "On the Numerical Problems of the Finite Element Methods," Symposium on Computer-Aided Engineering, University of Waterloo, Ontario, Canada, Study No. 5 (1970).

32. I. Fried, "Discretization and Round-Off Errors in the Finite Element Analysis of Elliptic Boundary Value Problems and Eigenvalue Problems," ScD thesis, Department of Aeronautics and Astronautics, MIT, June 1971.

33. O. Orringer, J.E. Kerwin, and R.M. Pelloux, "Failure and Safety Analysis of Controllable-Pitch Propellers," in Case Studies in Fracture Mechanics (T.P. Rich and D.J. Cartwright, ed.), U.S. Army Materials and Mechanics Research Center, Watertown, MA, AMMRC MS 77-5, June 1977.

34. B.M. Bailey, "Quartz-Window Design for Gas-Pressurized Photomultiplier Tube Installation," Journal of Nuclear Intruments and Methods, Vol. 125 (1973), 353-355.

35. O. Orringer and G. Stalk, "A Hybrid Finite Element for Stress Analysis of Fastener Details," Journal of Engineering Fracture Mechanics, Vol. 523 (1976).

36. Staff, "An Assessment of the Structural Modifications of the Grumman Flxible 870 Advanced Design Bus," DOT Transportation Systems Center, Cambridge, MA, March 1982.

37. J.H. Wilkinson, The Algebraic Eigenvalue Problem, Oxford University Press, London, 1965.

38. G. Dahlquist and Å. Björk, Numerical Methods, Prentice-Hall, Englewood Cliffs, NJ, 1974.

39. J.W. Givens, "Numerical Computation of the Characteristic Values of a Real Symmetric Matrix," Oak Ridge National Laboratory, Oak Ridge, TN, ORNL-1574, 1954.

40. S.B. Dong, J.A. Wolf, and F.E. Peterson, "On a Direct-Iterative Eigensolution Technique," International Journal of Numerical Methods in Engineering, Vol. 4 (1972), 155-161.

41. P. Tong, T.H.H. Pian, and L.L. Bucciarelli, "Mode Shapes and Frequencies by Finite Element Method Using Consistent and Lumped Masses," Computers & Structures, Vol. 1 (1971), 623-638.

42. J.S. Bendat, Principles and Applications of Random Noise Theory, Wiley, New York, 1958.

43. J.S. Bendat and A.G. Piersol, Random Data: Analysis and Measurement Procedures, Wiley, New York, 1971.

44. K.C. Park, "An Improved Stiffly Stable Method for Direct Integration of Nonlinear Structural Dynamics Equations," Journal of Applied Mechanics (June 1965), 464-470.

45. J.W. Leech, P.T. Hsu, and E.W. Mack, "Stability of a Finite-Difference Method for Solving Matrix Equations," AIAA Journal, Vol. 3 No. 11 (November 1965), 2172-2173.

46. R.E. Nickell, "On the Stability of Approximation Operators in Problems of Structural Dynamics," International Journal of Solids and Structures, Vol. 7 (1971), 301-319.

47. R.L. Bisplinghoff and H. Ashley, Principles of Aeroelasticity, Wiley, New York, 1962.

48. A.H. Wickens, "Steering and Dynamic Stability of Railway Vehicles," Journal of Vehicle System Dynamics, Vol. 5 (1975-76), 15-46.

49. H. Weinstock, "Analyses of Rail Vehicle Dynamics in Support of the Wheel/Rail Dynamics Research Facility," DOT Transportation Systems Center, Cambridge, MA, UMTA-MA-06-0025-73, June 1973.